https://doi.org/10.1016/j.conbuildmat.2022.129876

Roles of recycled fine aggregate and carbonated recycled fine aggregate in alkali-activated slag and glass powder mortar

Long Li [ab], Jianxin Lu [ab], Peiliang Shen [ab], Keke Sun [ab], Lance Edric Lou Pua[a], Jianzhuang Xiao [c], Chi Sun Poon *[ab]

a. Department of Civil and Environmental Engineering, The Hong Kong Polytechnic University, Hong Kong

b. Research Centre for Resources Engineering towards Carbon Neutrality, The Hong Kong Polytechnic University, Hong Kong

c. Department of Structural Engineering, Tongji University, Shanghai 200092, P.R. China

Abstract: Alkali-activated materials have attracted a lot of research interest due to the advantage of less CO_2 emission than ordinary Portland cement (OPC) systems. The use of recycled aggregate or carbonated recycled aggregate in new concrete is considered a good way to solve the problem of construction and demolition waste. This study aims to investigate the influences of recycled fine aggregate (RFA) and carbonated RFA (CRFA) on the properties of alkali-activated slag and glass powder mortar (AASGM). The macro properties (compressive strength, workability, setting time, and shrinkage) and microstructural properties of AASGMs prepared with RFA/CRFA were evaluated. The hydration evolutions of AASGMs and the reactions between RFA/CRFA and sodium silicate were investigated to explore the reaction mechanisms of AASGM with RFA/CRFA. The results showed that with the increase in RFA content from 0% to 100%, the flow value of AASGM decreased from 240mm to 145mm, the initial setting time was shortened by 44%, the 7 days autogenous shrinkage decreased by 82%, the 25 days drying shrinkage decreased by 31%, and the 28 days compressive strength firstly increased (RFA content ≤50%) and then decreased. On the contrary, with the increase in CRFA content from 0% to 100%, the flow value of AASGM increased from 240mm to 270mm, the final setting time increased by 37%, and the compressive strength decreased by 97%. The roles of RFA and CRFA in AASGM were different from their roles in OPC-based materials. That was because the calcium hydroxide in RFA could react with sodium silicate (SS) and increase the concentration of alkali, which accelerated the polymerization reaction of AASGM. However,

*Corresponding author. E-mail: cecspoon@polyu.edu.hk (C.S. Poon)

the calcium carbonate and silica gel in CRFA reacted with SS and reduced the concentration of alkali, and thus the polymerization reaction of AASGM was decelerated.

Keywords: Recycled fine aggregate; Carbonation; Alkali-activated mortar; Compressive strength; Shrinkage.

1. Introduction

Portland cement is one of the most frequently used construction materials today. However, a large amount of CO_2 is emitted during its manufacturing, which accounts for about 5%-8% of the global man-made CO_2 [1]. Researchers are trying to develop alternative materials for Portland cement to reduce carbon emissions. The production of alkali-activated materials, in which binders are sourced from industrial by-products and wastes such as slag, fly ash, silica fume, and glass powder, has a much lower carbon emission than Portland cement [2]. Moreover, alkali-activated materials have advantages of higher early strength, faster setting, and better chemical and fire resistances when compared to Portland cement materials [3][4][5]. Therefore, alkali-activated materials have been considered promising alternative materials to Portland cement, and many investigations have been conducted to promote the application of alkali-activated mortar or concrete.

In recent decades, the use of construction and demolition waste such as waste concrete as recycled coarse/fine aggregate to replace natural coarse/fine aggregate in Portland cement concrete/mortar has become a hot research topic. That is because it can alleviate the burden of waste disposal and save natural sources such as rock and river sand, which can bring in a good environmental benefit. However, the porosity of recycled aggregate (RA) was much higher than natural aggregate due to the presence of attached old mortar and initial cracks in the RA. As a result, the mechanical properties and durability of recycled aggregate concrete (RAC) are inferior to that of conventional concrete [6][7][8]. Therefore, the majority of RA is still used in non-structural concrete. When compared to recycled coarse aggregate (RCA), the old mortar content and water absorption of recycled fine aggregate (RFA) was higher [9], and there are more powder and more interfacial transition zones in RFA [10]. As a result, the mechanical properties and durability of concrete prepared with RFA deteriorated more significantly than when the same amount of RCA is incorporated [11]. And thus, the range of application of RFA is narrower than RCA and it is generally limited in low-strength mortar or concrete [9]. At present, several countries have recommended

the use of RCA in structural concrete, but RFA is not recommended [12]. Therefore, researchers in many countries are exploring to broaden the application of RA, especially FRA.

To explore the possibility of using RA in alkali-activated materials, some researchers studied the properties of alkali-activated concrete produced with RCA or RFA [13][14][15][16][17][18]. Hu et al. [15] and Tang et al. [19] reported that RCA reduces the workability and setting time of RAC and causes a reduction in mechanical properties. Huang et al. [16] revealed that using RFA as a replacement for river sand can improve the early strength of alkali-activated slag concrete, while at a later age the strength is still lower than that produced with river sand. However, because only limited research has been conducted in this field, the influences of RFA on the properties of alkali-activated mortar and the mechanism of how RFA influence the reactions remain unclear.

In recent years, the use of accelerated carbonation to modify RA for Portland cement concrete attracted increasing attention. The commonly used acceleration carbonation method could be classified into four types: there are four types [20][21]: 1. Standard carbonation method; 2. Pressurized carbonation method; 3. Flow-through carbonation method; 4. Wet carbonation. It has been considered a prospective method to absorb CO_2. Fang et al. [22] reported that after the RA with the size of 5-10 mm was treated by pressurized carbonation for 1 day, CO_2-sequestration could reach about 3% of RA by mass. Moreover, the use of carbonated RA can improve the mechanical properties and durability of RAC [20][21][23][24]. That is because the hydration products of cement in RA such as calcium silicate hydrates (C-S-H), $Ca(OH)_2$, and calcium aluminum sulfate can react with CO_2, and produce $CaCO_3$ and silica gel, which increases the solid volume of the adhered cement paste and thus reduces the porosity of RA [25][26]. As a result, the water absorption of RA is reduced, and the old interface transition zone (ITZ) in RA is enhanced after carbonation. Besides, the new ITZ between RA and new mortar is enhanced when using carbonated RA in RAC [27]. Because of the enhanced RA and new ITZ by carbonation, the mechanical properties and durability of RAC are enhanced. According to the literature, calcium carbonate may influence the reaction in alkali-activated material (AAM). Jeong et.al [28] investigated the use of precipitated $CaCO_3$ in the cementless CaO-

activated ground-granulated blast-furnace slag (GGBFS) system and found that precipitated $CaCO_3$ can improve the strength of this system because it can promote the dissolution of GGBFS. But Firdous et.al [29] reported that some calcium carbonate minerals could be reacted with sodium silicate to form sodium carbonate hydrate which had a negative effect on the strength of AAM. Therefore, CRFA may also have obvious influences on the properties of AAM, which is worthy to study. However, up to now, there is no study on the effect of using carbonated RFA (CRFA) in alkali-activated materials.

This study aims to investigate the influence of using RFA and CRFA to replace natural fine aggregate on the macro and microstructural properties of alkali-activated slag and glass powder mortar (AASGM), which is a typical alkali-activated mortar and has been comprehensively investigated in previous studies [30][31][32][33]. Moreover, the heat evolutions of AASGMs and the chemical reactions between the activator and RFA/CRFA will be studied to explore the reaction mechanisms of AASGMs with RFA/CRFA. The results of this study could provide a theoretical basis for using RFA and CRFA in AAMs.

2. Materials and methods

2.1 Materials

In this study, ground granulated blast-furnace slag (GGBS) and waste glass powder (GP) were utilized as precursors. The GGBS was commercially sourced from Mainland China. The GP was produced by grinding waste glass cullet, which was collected from a glass bottle recycling company in Hong Kong, with a laboratory ball mill. Before grinding, the waste glass cullet was cleaned with water and then dried in an oven at a temperature of 105℃ for two days. A Laser Diffraction Particle Size Analyzer was used to measure the particle size distribution of GP and GGBS, and the results are shown in Fig.1. The D50 of GP and GGBS were 15.73μm and 10.83μm, respectively. The apparent density of GGBS and GP were 2.87 g/cm^3 and 2.78 g/cm^3, respectively. A commercial powder-formed sodium silicate (SS) was used as the activator. The molar ratio (SiO_2/Na_2O) of the SS was 1.8. The chemical compositions of the raw materials were measured by X-ray fluorescence (XRF, Rigaku Supermini 200) and the results are listed in Table 1.

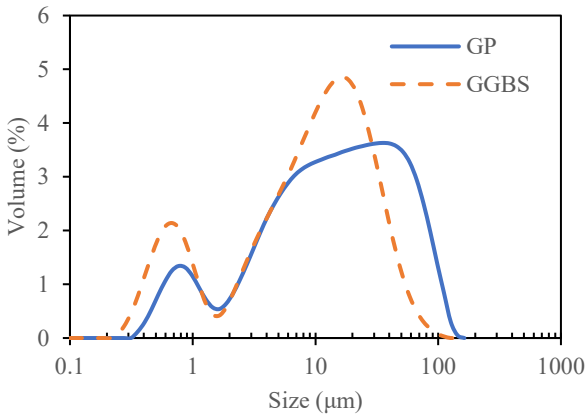

Fig. 1 Particle size distribution of GGBS and GP

River sand was used as the natural fine aggregate. Recycled fine aggregate (RFA) was produced by crushing Portland cement-based mortar cubes (150mm ×150mm ×150mm), which were prepared in the laboratory and cured in water for 3 months before crushing. A commonly used mix proportion (water: binder: sand= 0.5:1:3 by mass) [34] was used to cast the Portland cement-based mortar cubes for producing RFA. The cement used for producing the RFA was an ordinary Portland cement (OPC) CEM I 52.5 N and its chemical compositions are also shown in Table 1. The apparent density of the OPC was 3.09g/cm^3. The gradings of river sand and RFA are illustrated in Fig.2. The fineness modulus of river sand and RFA were 2.61 and 3.16, respectively. Compared to river sand, the average particle size of RFA was larger. It indicates that the specific surface area of RFA was smaller than river sand with the same volume. Part of RFA was carbonated using 99.9% industrial sourced CO_2 at a pressure of 1.0 bar for three days in a carbonation chamber. The carbonation method used was introduced in a previous study [23]. The fineness modulus of CRFA was considered as the same with RFA. The physical properties of river sand, RFA, and carbonated RFA (CRFA) were measured following BS EN 1907-6, and the results are shown in Table 2. It can be observed that after carbonation, the water absorption of RFA was reduced while the density was increased. The moisture contents of river sand, RFA and CRFA were considered as 0% because they were dried in an oven at 105℃ for 1 day before using.

Table 1 Chemical compositions of raw materials (GGBS, GP, SS, and OPC)

Chemical compositions	GP (% in mass)	GGBS (% in mass)	SS (% in mass)	OPC (% in mass)
Na_2O	15.40	0.00	35.80	0
MgO	1.60	7.90	0.21	0.86
Al_2O_3	2.20	17.20	0.61	5.63
SiO_2	68.90	35.10	62.90	18.50
P_2O_5	0.10	0.10	0.06	0.15
SO_3	0.12	2.18	0.08	3.84
K_2O	0.70	0.62	0.17	0.72
CaO	10.10	34.80	0.09	66.70
TiO_2	0	1.05	0	0.24
MnO	0.03	0.37	0	0.03
Fe_2O_3	0.65	0.50	0.04	3.05

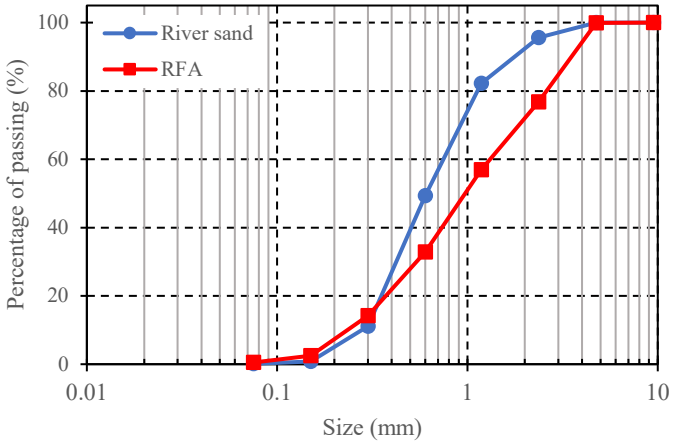

Fig. 2 Gradings of river sand and RFA

Table 2 Physical properties of river sand, RFA, and CRFA

	Water absorption (%)	Moisture content (%)	Mass ratio of additional water to aggregate (%)	Apparent Density (g/cm^3)	Particle density on an oven-dry basis (g/cm^3)	Particle density on a saturated surface-dry basis (g/cm^3)
River sand	0.3	0	0.3	2.696	2.665	2.667
RFA	8.03	0	8.03	2.515	2.092	2.260
CRFA	6.63	0	6.63	2.629	2.239	2.387

2.2 Mix proportions and specimens

The mix proportions of AASGMs prepared with RFA and CRFA are shown in Table 3. The control mix (M-control) was designed with adequate strength, setting time, and workability based on a previous study [31]. Specifically, the GP/GGBS ratio and the activator to precursor ratio were to make sure the mortar was not setting quickly and to have adequate strength (about 40MPa), while the water to precursor ratio was to make sure the mortar had adequate workability. Based on the control mix, river sand was replaced by RFA or CRFA with the same volume. Considering the water absorption of RFA and CRFA were higher than the river sand, additional water was added to make sure that the effective water to precursor ratio of the AASGMs was the same as that of M-control. As the aggregate was dried, the mass of additional water was equal to the mass of aggregate multiplied by its water absorption. The amount of effective water is equal to the amount of total water minus the amount of additional water.

Table 3 Mix proportions of AASGMs prepared with RFA and CRFA

Mix ID	Precursors		Water to precursor ratio	Effective water to precursor ratio	Activator to precursor ratio	Aggregate to precursor ratio		
	GP	GGBS				RFA	CRFA	River sand
M-Control	0.6	0.4	0.396	0.39	0.125	0	0	2.0
M-25%RFA	0.6	0.4	0.426	0.39	0.125	0.39	0	1.5
M-50%RFA	0.6	0.4	0.456	0.39	0.125	0.78	0	1.0
M-75%RFA	0.6	0.4	0.486	0.39	0.125	1.17	0	0.5
M-100%RFA	0.6	0.4	0.516	0.39	0.125	1.56	0	0
M-25%CRFA	0.6	0.4	0.422	0.39	0.125	0	0.417	1.5
M-50%CRFA	0.6	0.4	0.449	0.39	0.125	0	0.835	1.0
M-75%CRFA	0.6	0.4	0.475	0.39	0.125	0	1.252	0.5
M-100%CRFA	0.6	0.4	0.501	0.39	0.125	0	1.670	0

Before casting, the RFA, CRFA, and river sand were all dried in an oven at 105℃ for 1 day. The mortars were cast in a laboratory environment (RH ≈ 60%, T ≈ 23 ℃). After casting, the specimens were covered with plastic films and cured in molds for 72 hours before demolding to make sure that they had adequate strength to avoid damage during demolding. After demolding, the samples for compressive strength measurement were cured in sealed plastic bags to prevent moisture loss until testing, rather than in water or an unsealed ambient environment. That was because the compressive strength of alkali-activated slag

was higher by curing in sealed plastic bags than by curing in water and unsealed environment [35][36]. The curing conditions for other tests will be introduced in the section on test methods.

2.3 Test methods

The experimental programme of this study is shown in Fig.3. First, the macro properties, micro properties, and heat evolution of AASGM with RFA and CRFA were studied. Then, to explain the influence of RFA and CRFA, the reactions between RFA/CRFA and sodium silicate (SS) were studied by analyzing the compositions of the formed gel, the solution, and the RFA/CRFA after soaking RFA/CRFA in SS solution for a period. The detailed test methods will be introduced below.

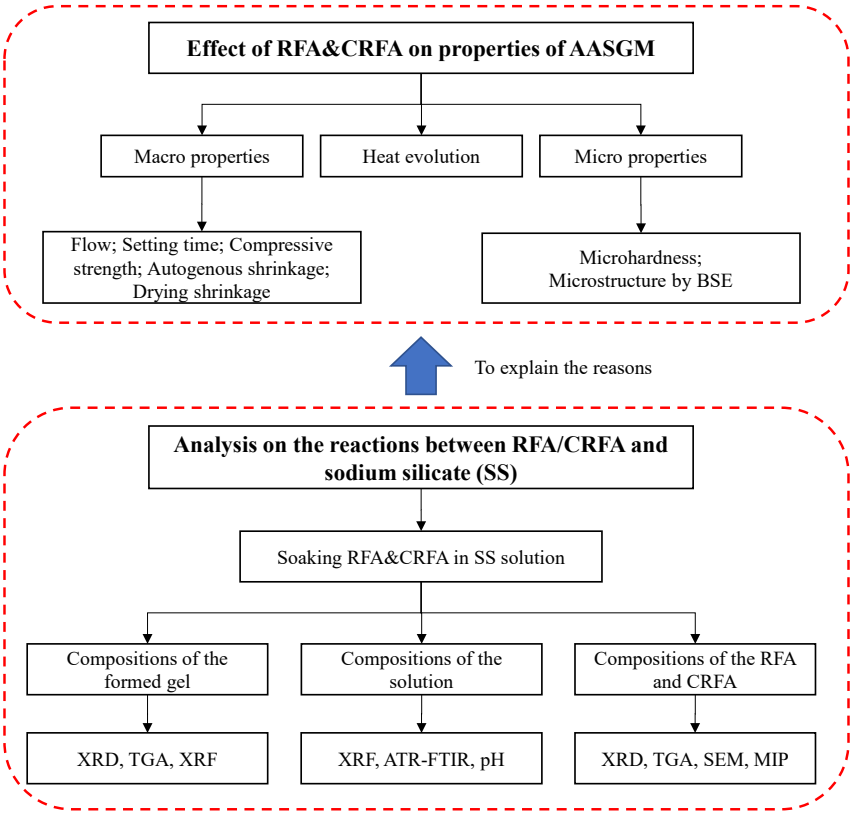

Fig. 3 Experimental programme of this study

2.3.1 Measurement of macro properties of AASGMs

(1) Flow

The flow values of fresh AASGMs were measured with a flow table in accordance with BS EN 1015-3. The flow value is defined as the mean diameter of fresh mortar placed on the flow table disc after 25 vertical impacts by raising the flow table.

(2) Setting time

Initial and final setting times of the fresh AASGMs were measured by using a Vicat apparatus according to BS EN 480-2. The initial and final setting times are defined as the time from the addition of water to the moments at which the distance between the needle and the base plate is 4 mm and 25mm, respectively.

(4) Compressive strength

Compressive strength of AASGMs at the age of 3 days, 7 days, and 28 days were measured based on BS EN 1015-11Three cubic samples with a size of 40mm×40mm×40mm were prepared for measuring the compressive strength of each mix at each age. The loading rate was set as 0.6 MPa/s.

(5) Autogenous shrinkage

Autogenous shrinkage of AASGMs was measured based on ASTM C1698-19. First, the fresh mortar was filled into a plastic corrugated tube with a size of Φ29mm×420 mm and sealed with two end plugs to avoid moisture loss. Then, the mortar was stored horizontally in a room at a temperature of 23±1 ℃. Finally, the length of the mortar was measured by using a digital gauge with a solution of 0.001mm at regular intervals for up to 14 days. The autogenous shrinkage at a specific time was defined as the change in length divided by the original length of the specimen at the final setting.

(6) Drying shrinkage

Drying shrinkage of AASGMs was measured in accordance with ASTM C596. The size of the sample for the drying shrinkage test was 25mm×25mm×280mm. After demolding, each sample was soaked in $Ca(OH)_2$ saturated solution for two days. After removal from the solution, the surfaces of the sample were wiped surface dry using towels and the length of the sample was considered as the original length. Then,

the sample was placed in an environmental chamber at a relative humidity of 50% and temperature of 25℃. The lengths of the samples at specific ages were recorded using a length comparator up to 25 days. The drying shrinkage at specific ages was defined as the change in length divided by the original length of the specimen.

2.3.2 Evaluation of microstructural properties of AASGMs

(1) Measurement of microhardness

Two specimens with the size of about 20mm×20mm×10mm for each mix were prepared for microhardness testing by cutting from a mortar cube (40mm×40mm×40mm). The samples were soaked in ethanol for 1 day and then dried in a vacuum chamber at 40℃ for 7 days to stop further reactions of mortar. This ethanol-pretreated drying method have been commonly used to stop the hydration of cementitious materials [37]. After drying, the samples were impregnated with epoxy resin in cylindrical molds with a diameter of 30mm. Next, one surface of the samples was polished by using a polishing machine (Buehler AutoMet 250). The detailed procedures for polishing were introduced in previous studies [38][39]. After polishing, the samples were stored in a vacuum chamber at 40℃ for 7 days before testing.

The microhardness of AASGMs was measured by using a digital Vickers micro-hardness tester (HVX-1000A). To consider the heterogeneous properties of mortar, the microhardness values in three randomly selected testing zones were measured for each mortar. Every testing zone was located near the aggregate-new paste interface, and thus the microhardness of both the aggregate and new paste can be evaluated. In each testing zone, the indentation points were located at specified distances from the aggregate-new paste interface, and there were 5 indentation points at each distance.

(2) Observation of microstructure

The microstructures of AASGMs with RFA and CRFA were observed under the backscattered electron (BSE) mode in SEM (Tescan VEGA3). For each mix, one of the samples that used in the microhardness test was selected for observation under the BSE. Before testing, the samples were dried in a vacuum chamber at 40℃ for 7 days and then coated with a layer of gold.

205 **2.3.3 Measurement of heat evolution of AASGMs with RFA and CRFA**

206 The heat evolutions of AASGMs prepared with RFA and CRFA were recorded by using an isothermal
207 calorimeter (Calmetrix I-Cal 4000). The mass of precursors of each mix for the test was controlled as 15.0g.
208 After mixing for 4min, the fresh mortar was put into the calorimeter immediately and the heat release was
209 recorded for more than 5 days.

210 **2.3.4 Exploration of chemical reactions between SS with RFA/CRFA**

211 To study the influence of RFA/CRFA as a replacement of river sand on chemical reactions in AASGMs,
212 the reactions between RFA/CRFA and SS solution were investigated. To achieve this, RFA and CRFA
213 were firstly soaked in SS solution for two days. Here, the SS solution without RFA/CRFA (SS-control) was
214 used as the control. The SS solutions soaked with RFA and CRFA were marked as SS-RFA and SS-CRFA,
215 respectively. The mass proportions of the constituents in the soaking tests are shown in Table 4. Then, the
216 RFA, CRFA, SS solution, and the gel formed in SS solution after soaking for two days were characterized
217 by using the following techniques.

218 Table 4 Mass proportions of constituents in soaking test

ID	Mass (g)			
	SS	Water	RFA	CRFA
SS-control	20	200	0	0
SS-RFA	20	200	100	0
SS-CRFA	20	200	0	100

219 **(1) Methods for characterization of RFA and CRFA after soaking in SS solution**

220 Thermal gravimetric analysis (TGA, Rigaku - Thermo plus EVO2) and X-ray diffraction analysis (XRD,
221 Rigaku SmartLab 9kW - Advance) was used to analyze the changes in compositions of RFA and CRFA
222 after soaking in SS solution for two days. To prepare the samples, RFA/CRFA particles before and after
223 soaking in the SS solution were soaked in ethanol to stop the further reaction, dried in a vacuum chamber
224 at 40℃ for two days, and then ground to powder (< 75μm). Next, these samples were stored in a vacuum
225 chamber at 40℃ for 7 days before testing.

The morphologies of the RFA and CRFA after soaking in SS solution were observed under scanning electronic microscopy (SEM, Tescan VEGA3) with energy-dispersive X-ray spectroscopy (EDS). Before testing, the RFA and CRFA particles were dried in a vacuum chamber at 40℃ for 7 days and coated with gold.

The pore size distributions of the RFA and CRFA after soaking in SS solution were determined by using mercury intrusion porosimetry (MIP, Micromeritics AutoPore IV 9500). The RFA and CRFA with particle sizes between 2.36mm and 5.00mm were used in the test and the samples were placed in a vacuum chamber at 40℃ for 7 days before testing.

(2) Methods for characterization of SS solution after soaking with RFA and CRFA

The chemical compositions of SS solution before and after soaking with RFA/CRFA were measured by using XRF. The pH values of SS solution in SS-control, SS-RFA, and SS-CRFA at specified moments were measured by using a pH meter for up to 7 days. The functional groups of SS solution in the SS-control, SS-RFA, and SS-CRFA were evaluated by using attenuated total reflection-Fourier transform infrared spectroscopy (ATR-FTIR).

(3) Methods for characterization of the gel formed in SS solution

The gel formed in the SS solution was separated from the SS solution by centrifugal method and dried in a vacuum-dry chamber at 40℃ for 7 days. Then, the sample was ground into powder and stored in a vacuum chamber for 7 days before testing. The XRF, TGA, and XRD techniques were used to analyze the compositions of the gel.

3. Test results

3.1 Macro properties of AASGMs with RFA and CRFA

3.1.1 Flow value

The flow values of AASGMs with RFA and CRFA are shown in Fig.4. The results show that the flow of AASGM decreased with the increase of RFA content. It can be speculated that this reduction was not caused by the difference in specific surface area and water absorption of fine aggregate. On one hand, the average

particle size of RFA was larger than river sand according to Fig. 2, and thus the specific surface area of RFA was smaller under the same volume. Generally, a smaller specific surface area of fine aggregate leads to a higher flow of mortar. On the other hand, additional water has been added to the mixture to consider the higher water absorption of RFA, and thus it will not lead to a decrease in flow. It was reported [40] that the slump of OPC-based concrete with recycled aggregate was higher than that without recycled aggregate when additional water had been added. Therefore, it should be due to the reaction between RFA and alkali activator that caused the reduction in the flow of AASGM. It was possible that after incorporating RFA in AASGM, $Ca(OH)_2$ in RFA was dissolved into the new paste quickly and reacted, which increased the alkali concentration in AASGM and thus accelerating the polymerization reaction in AASGM. This feature will be confirmed by the results in section 3.3 and section 3.4. Generally, the workability of alkali-activate slag is reduced with an increase in Na_2O/SiO_2 ratio (or alkali concentration) [41].

However, the flow value of AASGM increased with the increase of CRFA content. One reason was that the old mortar at the surface layer of CRFA was denser than RFA [21][42], and thus SS solution was more difficult to penetrate into CRFA at an early age. It was reported that water is more difficult to transport in carbonated recycled aggregate than in un-carbonated one [43]. It means CRFA might not be saturated initially and thus the liquid content in the new paste of AASGMs with CRFA would be higher than that of M-control. Another possible reason was that CRFA decelerated the reactions in AASGM, which can be reflected in the results of setting time and heat evolution below.

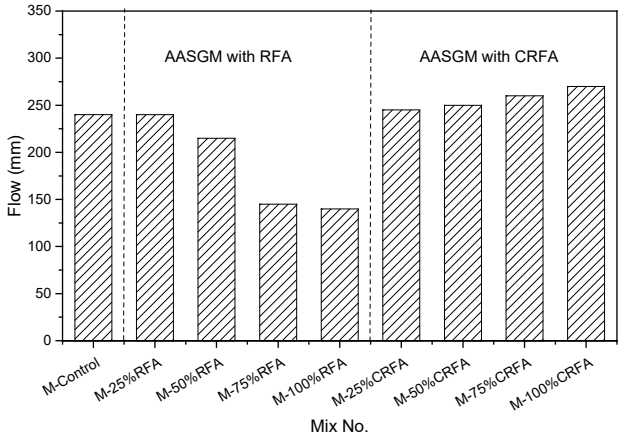

Fig. 4 Flow values of AASGMs with RFA and CRFA

3.1.2 Setting time

The setting time of AASGMs with RFA and CRFA is shown in Fig.5. The initial setting time of AASGM decreased with the increase of RFA content. This result was consistent with that reported by Tang and Li [44]. It should be also related to the dissolution of $Ca(OH)_2$ from RFA, which increased the alkali concentration of the activator and accelerated the polymerization reaction. However, the final setting time of AASGM decreased firstly and then increased with the increase of RFA content. It may be related to the change in the alkali concentration of the system. Generally, the setting time of alkali-activate materials decreases firstly and then increases with the increase of alkali concentration [45][46].

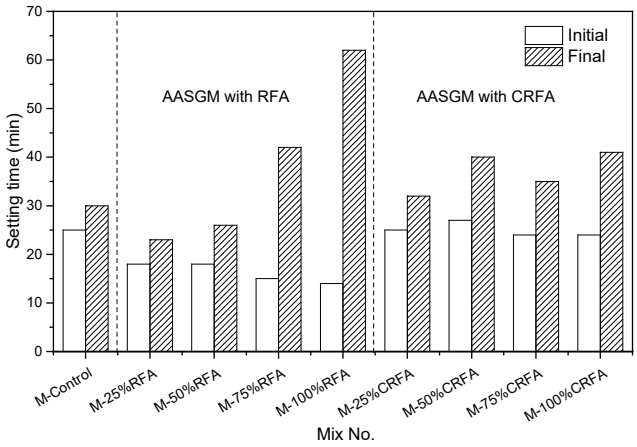

Fig. 5 Setting time of AASGMs with RFA and CRFA

From Fig.5, the initial setting time of AASGM did not show an obvious change as CRFA content increased, while the final setting time increased with the increase of CRFA content. It indicates that CRFA decelerated the polymerization reaction of AASGM. It may be because some phases in CRFA such as calcium carbonate and silica gel had reacted with the alkali activator and thus reduced the alkali concentration of the activator. This speculation will be confirmed in section 3.4.

3.1.3 Compressive strength

The compressive strength of AASGMs with RFA and CRFA at the age of 3 days, 7 days, and 28 days are shown in Fig. 6. It shows that the compressive strength of AASGM first increased and then decreased with the increase of RFA content, and the optimum RFA content was 50% at the age of 28 days. This

phenomenon was different from the case of OPC-based mortar or concrete, in which the strength continuously decreases with the increase of RFA content because RFA is weaker than river sand [47][48]. That was because RFA could accelerated the polymerization reactions of AASGM and thus enhance the new paste of AASGM, which will be confirmed by microhardness results. However, when too much RFA was incorporated, the adverse effect on compressive strength caused by weaker RFA over river sand outweighed the above positive effects. As a result, the 28^{th}-day compressive strength of AASGM reduced with the increase of RFA content when it was higher than 50%. In addition, the 3 days compressive strength of AASGM with RFA reached the maximum when the RFA content was 100%, while the 7 days compressive strength of AASGM with RFA was the highest when the RFA content was 70%. It indicates that incorporating RFA accelerated the development of the early strength of AASGM.

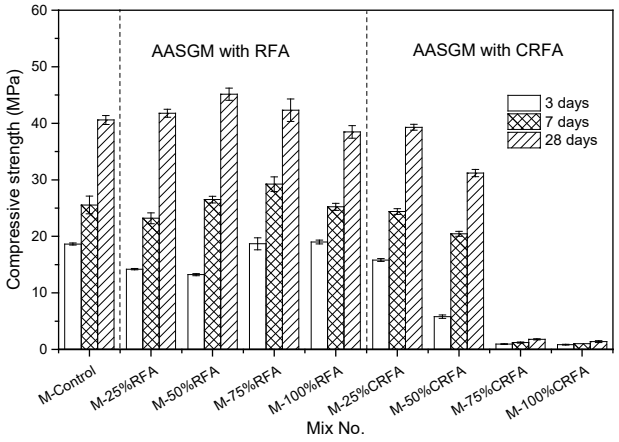

Fig. 6 Compressive strength of AASGMs with RFA and CRFA

From Fig.6, it can also be observed that the compressive strength of AASGM decreased with the increase of CRFA content. Also, the compressive strength of AASGM with CRFA was lower than that using the same amount of RFA. This tendency was contrary to the use of RFA and CRFA in cement mortar. Generally, the compressive strength of cement mortar prepared with CRFA is higher than that of using the same amount of RFA due to the enhancement of RFA by carbonation [26]. In this study, when the CRFA content was higher than 75%, the compressive strength of AASGM was very low (< 2.0MPa). It was because some phases in CRFA such as calcium carbonate and silica gel could deplete part of the alkali activator as described above, and thus it reduced the polymerization degree of C-(N)-A-S-H in AASGM. Generally, the

compressive strength of alkali-activated slag materials is positively related to the polymerization degree of C-A-S-H gels [49]. Therefore, the compressive strength was AASGM was reduced after incorporating CRFA.

3.1.4 Autogenous shrinkage

The autogenous shrinkage values of AASGMs with RFA and CRFA are presented in Fig. 7. It shows that the autogenous shrinkage of AASGM decreased significantly with the increase of RFA content. It means that the use of RFA is an effective way to reduce the autogenous shrinkage of AASGM. This feature is similar to that in OPC system, which showed that the autogenous shrinkage of concrete or mortar decreases with the increase of RFA content [50][51]. The main reason for this phenomenon was the internal curing effect of RFA [14], rather than the accelerated polymerization reaction which could lead to increased autogenous shrinkage [52]. Specifically, RFA would absorb part of the water from the new paste at an early age and release water to the new paste during its reaction process. As a result, the volume reduction of the new paste was smaller. Moreover, because of the internal curing effect of RFA, a little expansion occurred in M-100%RFA at the early ages, which is similar to the case of using lightweight aggregate in alkali-activated mortar. Sakulich and Bentz [53] also observed the expansion phenomenon in waterglass/NaOH-activated slag mortar when using lightweight aggregate (an aluminosilicate clay).

The autogenous shrinkage of AASGM also decreased with the increase of CRFA content. However, AASGM with CRFA had a lower autogenous shrinkage than that with a similar amount of RFA. Especially, the autogenous shrinkage values of AASGM with 75% and 100% CRFA were negative. It indicates that except for the internal curing effect of CRFA, the chemical reactions also contributed to the smaller autogenous shrinkage of AASGM with CRFA. One possible reason was that CRFA reduced the alkali content of the activator and thus reduced the formation of the C-(N)-A-S-H gel.

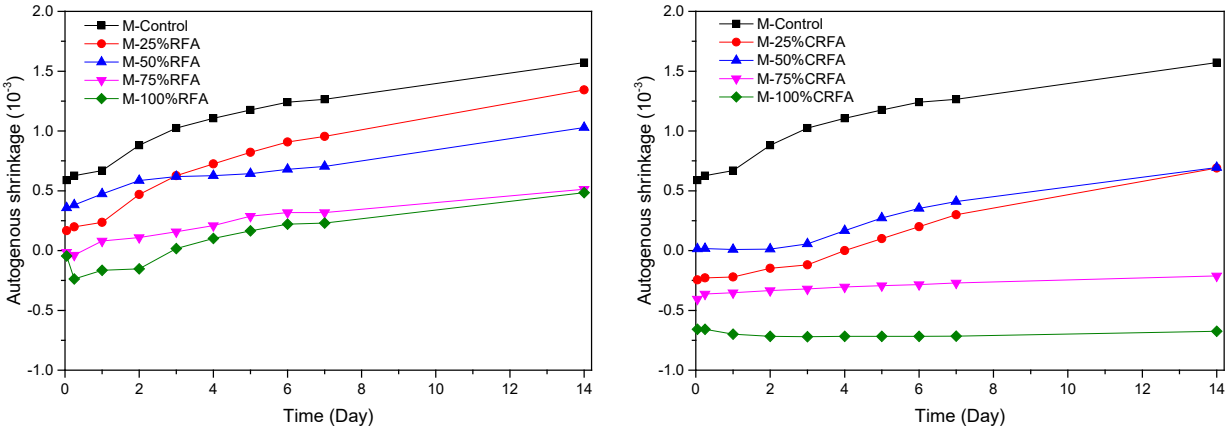

(a) (b)

Fig. 7 Autogenous shrinkage of AASGMs with RFA (a) and AASGMs with CRFA (b)

3.1.5 Drying shrinkage

The drying shrinkage values of AASGM with RFA and CRFA are illustrated in Fig. 8. The drying shrinkage of AASGM decreased with the increase of RFA content, which is different from the case in OPC systems. It was reported [48] that the drying shrinkage of cement mortar increases with the increase of RFA content. There are two possible reasons for this feature. First, incorporating RFA increased the alkali concentration of the activator in AASGM, which was equivalent to reducing SiO_2/Na_2O of sodium silicate. Gao et.al [54] revealed that drying shrinkage of alkali-activated slag-fly ash composites increased with the increase of SiO_2/Na_2O of activator due to refined pore structure caused by increased SiO_2/Na_2O. Second, like autogenous shrinkage, the internal curing effect of RFA can also offset part of drying shrinkage. Moreover, with the increase of RFA content, the drying shrinkage of AASGM developed more slowly at early ages. For example, the 1-day drying shrinkage of M-control was about 95% of 25-day shrinkage, while the 1-day drying shrinkage of M-100%RFA was only about 15% of 25-day shrinkage. It was also because of the internal curing effect of RFA, which can offset the water loss in the paste at an early age.

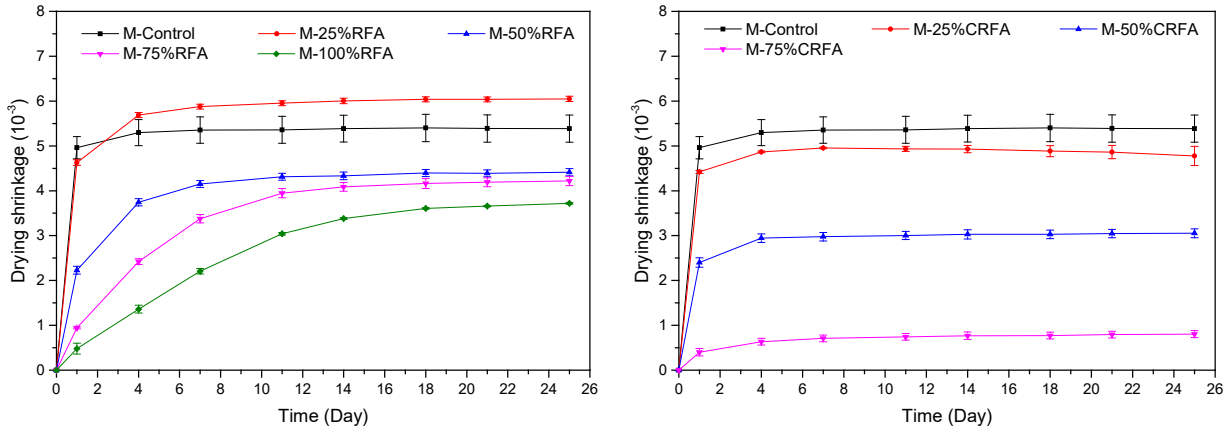

(a) (b)

Fig. 8 Drying shrinkage of AASGMs with RFA (a) and AASGMs with CRFA (b)

From Fig. 8, it can also be found that the drying shrinkage of AASGM also decreased significantly with the increase of CRFA content and the reduction was even larger than that using RFA. One reason was the large expansion of AASGM with CRFA as stated above, which can offset its drying shrinkage. Moreover, CRFA caused a reduction of the alkali concentration in the activator, which is another reason for the decrease in drying shrinkage of AASGM. It was reported that the drying shrinkage of alkali-activated slag decreased with the decrease of alkali concentration [55-56]. That is because with the decrease of alkali concentration, the polymerization degree decreased and less C-(N)-A-S-H gel was produced, which means the number of gel pores was reduced. Collinsa and Sanjayan [57] reported that the drying shrinkage of alkali-activated mortars was mainly dependent on the loss of water from the mesopores (1.25nm to 25 nm) rather than the larger pores. Therefore, the reduced polymerization degree by CRFA also contributed to the decrease in drying shrinkage of AASGM.

3.2 Microstructural properties of AASGMs with RFA and CRFA

3.2.1 Microstructure

The BSE images of AASGMs (M-Control, M-100%RFA, and M-100%CRFA) are shown in Fig. 9. It can be seen there are a lot of unreacted GGBS and GP particles in the new paste of all the samples. In the M-100% RFA, no obvious difference was found in the new paste when compared with the M-control, but

there was a layer of old cement paste attached to the RFA and initial cracks were observed between the river sand and the old cement paste. Moreover, the width of the initial cracks between the river sand and the old cement paste was larger than that between the old cement paste and the new paste. It indicates that the bonding strength of the old cement paste-river sand interface should be inferior to the old cement paste-new paste interface. In M-100% CRFA, the cracks between the river sand and the old cement paste were smaller than that in M-100%RFA. That was because $Ca(OH)_2$ and C-S-H reacted with CO_2, producing $CaCO_3$ particles which are larger in volume. As a result, the cracks can be partially filled. However, in the M-100%CRFA, there were much more pores in the new paste than in the M-control and M-100%RFA, which indicated that the new paste in M-100%CRFA was much weaker than M-control. It can be speculated that the addition of CRFA had a negative effect on the polymerization process in AASGM.

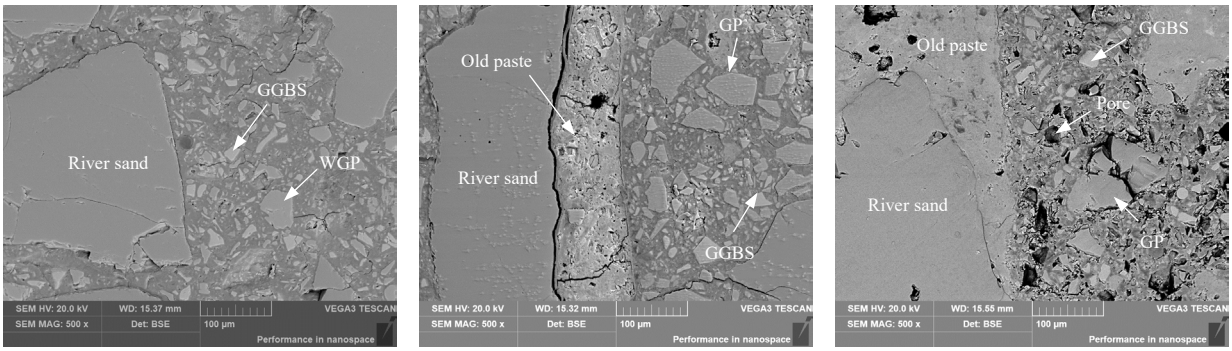

(a) (b) (c)

Fig. 9 BSE images of AASGMs. (a) M-Control; (b) M-100%RFA; (c) M-100%CRFA

3.2.2 Microhardness

The microhardness results of AASGMs with RFA and CRFA at the zone near the aggregate-new paste interface are shown in Fig. 10. It was observed that in each AASGM, the microhardness of the new paste and the old paste at the surface layer of RFA/CRFA changed little when the distance from the interface varied. However, they changed a lot in different AASGMs. To have a better understanding, the average microhardness of the old paste at the surface layer of RFA/CRFA and the new paste in different AASGMs are displayed in Table 5. To make a comparison, the average microhardness values of the old paste at the surface layer of RFA and CRFA are also given in Table 5.

Table 5 Average microhardness results

Mix ID or aggregate ID	Old paste at the surface layer of RFA/CRFA		New paste	
	Average microhardness (HV0.01)	SD	Average microhardness (HV0.01)	SD
M-Control	n.a.	n.a.	50.5	10.3
M-50%RFA	35.9	3.0	58.8	10.3
M-100%RFA	35.9	9.3	65.7	14.4
M-50%CRFA	67.7	12.8	47.5	7.7
M-100%CRFA	62.6	17.4	25.8	5.2
RFA	31.2	6.2	n.a.	n.a.
CRFA	62.1	18.2	n.a.	n.a.

Note: n.a. is not available.

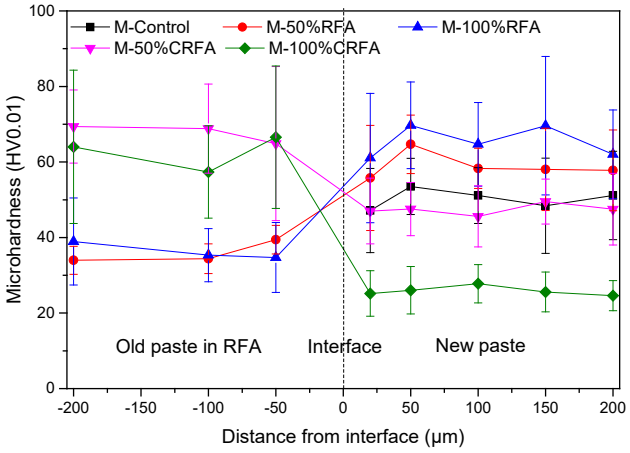

Fig. 10 Microhardness of AASGMs with RFA and CRFA

From Table 5, it is observed that as more RFA was incorporated, the microhardness of the new paste in AASGM was higher. It indicates that the new paste in AASGM could be enhanced by incorporating RFA. That was because the $Ca(OH)_2$ in RFA could be dissolved into new paste and increase the alkali content of activator, which accelerated the polymerization reaction of new paste. That was why the compressive strength of AASGM increased when less than 50% of RFA was incorporated. However, because RFA was weaker than river sand and it has a negative effect on compressive strength, the compressive strength of M-100%RFA was lower than M-control although the microhardness of new paste in M-100%RFA was higher. Moreover, the microhardness of the old paste at the surface layer of RFA in AASGM was higher than that

of the original RFA. It indicates that the reaction between RFA and alkali activator also leads to denser old paste on RFA.

On the contrary, the microhardness of new paste in AASGM decreased with the increase of CRFA content. It explains why the compressive strength of AASGM decreased significantly with the increase of CRFA content and the compressive strength of AASGM with CRFA was lower than the AASGM with the same percentage of RFA although CRFA was stronger than RFA. It indicates that the reaction between CRFA and alkali activator had a negative effect on the polymerization process in the new paste of AASGM. That was because the calcium carbonate and silica gel in CRFA reacted with the alkali activator and decreased the alkali concentration of activator. In addition, the microhardness of the old paste at the surface layer of CRFA in AASGM was close to that of the original CRFA, which was much higher than that of RFA due to carbonation. It indicates that when incorporating CRFA in AASGM, the obviously weakened new paste is the key to influencing the mechanical properties of AASGM with CRFA.

3.3 Heat evolutions of AASGMs with RFA and CRFA

The heat flow and cumulative heat curves of AASGMs with RFA and CRFA are shown in Fig. 11. There are three main peaks in the heat flow curve of M-control. Based on some literature [30][53][58], the initial peak within 20min was produced due to the wetting and dissolution of the SS powder and the precursors. The second peak between 0.6h and 6h represented the precipitation of C-(N)-A-S-H gel on the surface of GGBS and GP particles. But these gels as a protective layer hindered the further reaction of GGBS and GP, which contributed to the decreased heat flow after the second peak and the long induction period after 6h. After the induction period, the protective layer was continuously destroyed, and thus the hydration accelerated, which contributed to the third peak.

After incorporating RFA in AASGM, the second peak in the heat flow curve was absent. It is because the $Ca(OH)_2$ in RFA was dissolved into the new paste, which increased the hydroxide concentration in the activator and accelerated the reactions. As a result, the second peak and the first peak were merged into one peak. It was also reported in the literature [59][60] that with the decrease of SiO_2/Na_2O or increase of

hydroxide concentration in SS, the second peak in the heat flow curve of alkali-activated slag gradually disappeared. With the increase of RFA content, the third peak of heat flow of AASGM appeared earlier and the intensity increased. Meanwhile, the cumulative heat of AASGM was increased with the increase of RFA. It indicated that the polymerization process was accelerated, and more reaction product was generated in AASGM after incorporating RFA. It explained the phenomenon that with the increase of RFA content, the flow value of AASGM decreased, the initial setting time decreased, and the microhardness of new paste in AASGM increased.

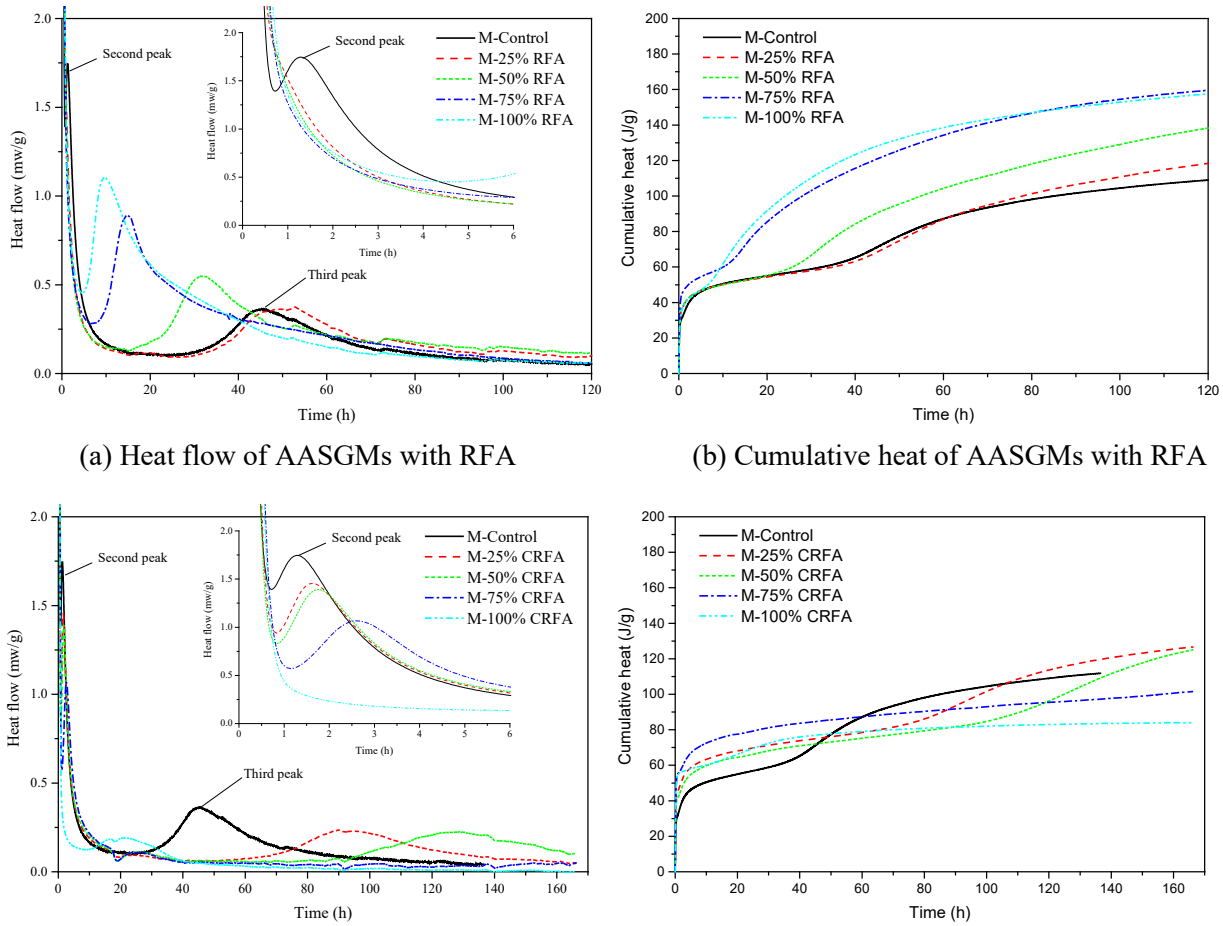

(a) Heat flow of AASGMs with RFA (b) Cumulative heat of AASGMs with RFA

(c) Heat flow of AASGMs with CRFA (d) Cumulative heat of AASGMs with CRFA

Fig. 11 Heat flow and cumulative heat of AASGMs with RFA and CRFA

With the increase of CRFA content in AASGM, the appearance of the second peak of heat flow was delayed. It is different from the case of incorporating RFA. Moreover, the appearance of the third peak was

also significantly delayed. The third peak of the control, 25%CRFA and 50%CRFA were at times of 47h, 96h, and 135h. For 75%CRFA and 100%CRFA, the second peak did not appear before 7 days. In addition, the peak heat flow and the cumulative heat decreased with the increase of CRFA content. It indicates that the polymerization process in AASGM was decelerated after incorporating CRFA. It explained the phenomenon that with the increase of CRFA content, the flow value and setting time of AASGM increased, while the microhardness of new paste in AASGM decreased. Also, because of the decelerated polymerization process, the autogenous shrinkage of AASGM with CRFA was lower than AASGM with the same percentage of RFA.

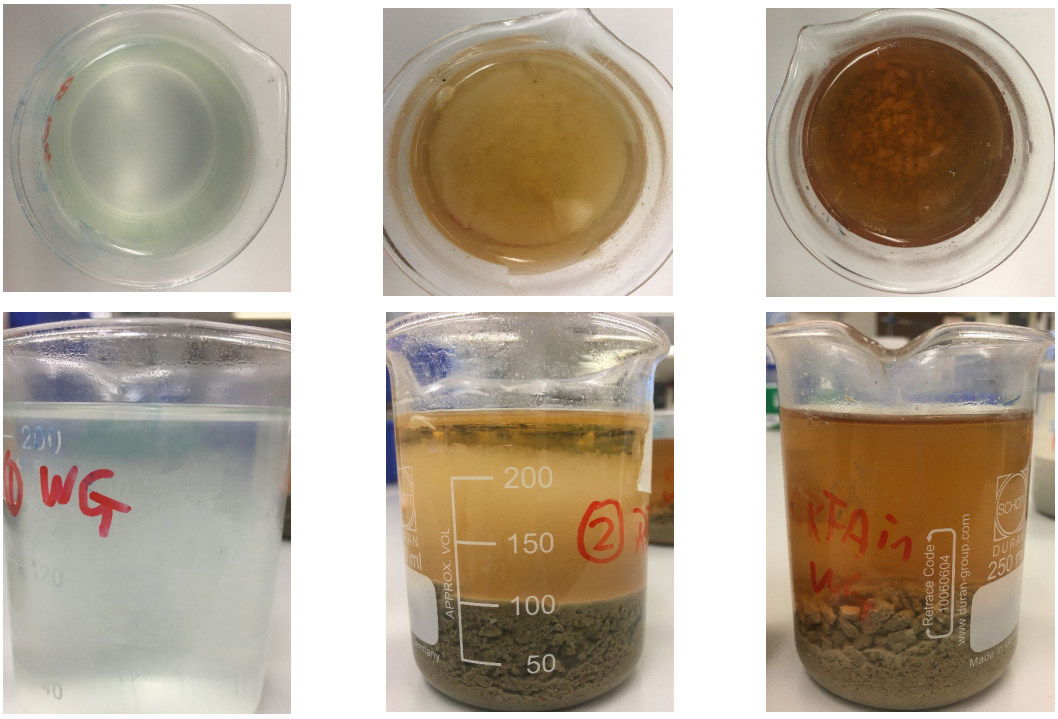

(a) SS-control (b) SS-RFA (c) SS-CRFA

Fig. 12 Photos of SS solutions after soaking with RFA/CRFA for 1 day

3.4 Chemical reactions between SS solution and RFA/CRFA

To further explore how RFA and CRFA influence the chemical reactions in AASGM, the reactions between SS solution and RFA/CRFA were investigated. Fig. 12 shows the photos of the SS solutions after soaking with RFA or CRFA (SS-control, SS-RFA, and SS-CRFA) for 1 day. It is observed that a lot of gel

452 was formed in SS-RFA. It means that some substances from RFA were dissolved into SS solution and
453 reacted. But there was no visible gel formed in SS-CRFA. Moreover, when SS-CRFA was vibrated gently
454 by hand, small gas bubbles were observed, which was similar to the phenomenon of carbonated water.
455 Therefore, it is inferred that CO_2 gas might be formed in the SS-CRFA. To reveal the chemical reactions
456 between RFA/CRFA and SS solution, the characteristics of SS solution, RFA, CRFA, and the gel formed
457 in the SS-RFA after the soaking test were further analyzed.

458 **3.4.1 Characteristics of the gel formed in the SS-RFA**

459 **(1) XRF**

460 The chemical compositions of the gel formed in the SS-RFA are shown in Table 6. The main
461 compositions in the gel formed in SS-RFA are Na_2O, SiO_2, and CaO. It indicates that the $Ca(OH)_2$ in RFA
462 might have been dissolved into SS solution and reacted with SS. It had been reported that $Ca(OH)_2$ can
463 react with sodium silicate (SS) in the presence of water to form a C-S-H gel [61]. Moreover, small amounts
464 of Al_2O_3, SO_3, MgO, and Fe_2O_3 also were also present in the gel. It indicates that the calcium aluminate
465 sulfate in RFA such as ettringite and mono sulfate had been also dissolved into SS solution and reacted
466 with SS. Based on chemical compositions, the gel formed in SS-RFA should be sodium-containing calcium
467 aluminosilicate hydrates (C-(N)-A-S-H).

468 Table 6 Chemical compositions of the gel formed in SS-RFA

	Chemical compositions of the gel									
	Na_2O	MgO	Al_2O_3	SiO_2	P_2O_5	SO_3	Cl	K_2O	CaO	Fe_2O_3
% in Mass	30.40	0.41	2.00	52.20	0.09	1.66	0.08	0.88	11.70	0.54

469

470 **(2) XRD**

471 The XRD pattern of the gel is shown in Fig. 13. There is a broad band between 20° to 37° and the peak
472 is at 29.4°, which might be related to the existence of C-(N)-A-S-H gel. Moreover, there is a peak at 37.6°.
473 It could be assigned as hydrotalcite (magnesium aluminum hydroxide), which is usually detected in alkali-
474 activated slag materials [62]. In addition, the peaks at 20.9° and 26.6° are associated with quartz which is
475 due to the presence of residual river sand in RFA.

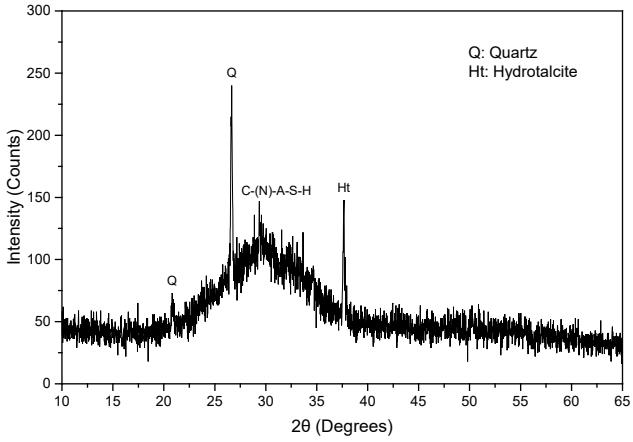

Fig. 13 XRD pattern of the gel formed in SS-RFA

(3) TGA

The TG and DTG results of the gel formed in SS-RFA are shown in Fig. 14. Based on the TGA results of alkali-activated slag materials reported by Zuo et al [63], the first peak from 30℃ to 140℃ is related to the dehydration of C-(N)-A-S-H, while the second peak from 250℃ to 450℃ corresponds to the decomposition of hydrotalcite. The third peak from 600℃ to 850℃ is related to the decomposition of calcium carbonate due to atmosphere carbonation. Combining the above XRF, XRD, and TGA results, it can be inferred that when soaking RFA in SS solution, the $Ca(OH)_2$ and calcium aluminate sulfate in RFA were dissolved and reacted with SS, producing C-(N)-A-S-H gel and hydrotalcite.

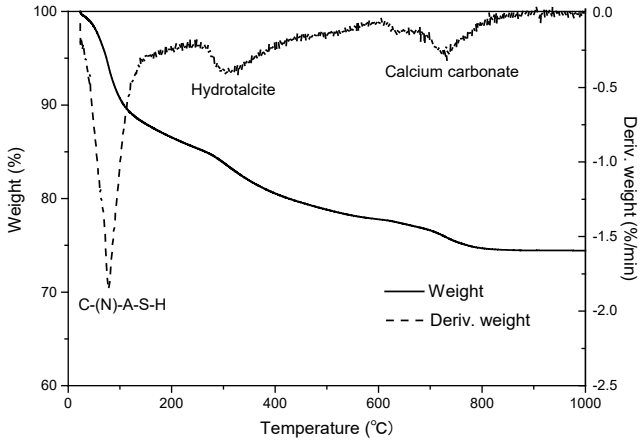

Fig. 14 TG results of the gel formed in SS-RFA

3.4.2 Characteristics of RFA and CRFA after soaking in SS solution

(1) XRD

The XRD results of RFA/CRFA before and after soaking in SS solution for 1 day are shown in Fig. 15. The main crystalline phases in RFA were quartz, $Ca(OH)_2$, calcite, and C-S-H. The main minerals in RFA after soaking in SS solution were similar to the original RFA. But the intensity of the peaks corresponding to $Ca(OH)_2$ was reduced. It indicates that part of $Ca(OH)_2$ in RFA reacted with SS solution. Quartz and calcite were observed in CRFA, which was similar to that of CRFA after soaking in SS solution.

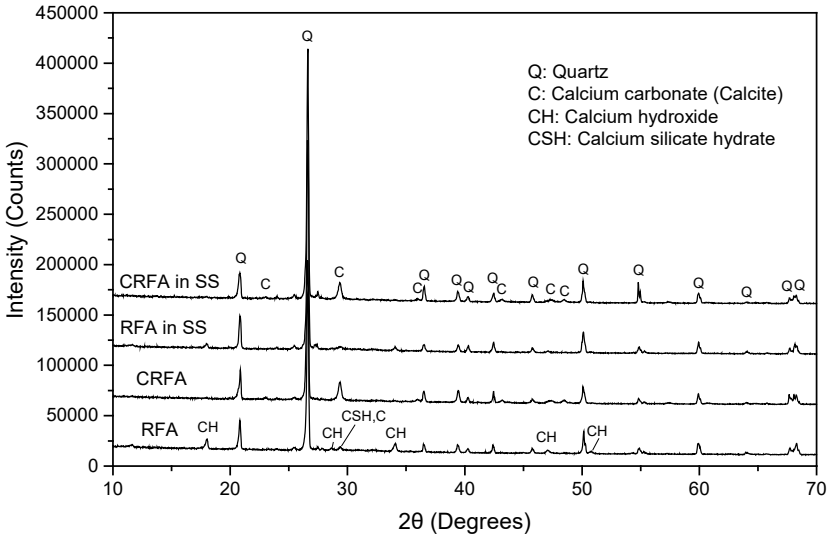

Fig. 15 XRD patterns of RFA/CRFA before and after soaking in SS solution

(2) TGA

The TG and DTG results of RFA/CRFA before and after soaking in SS solution for 1 day are shown in Fig. 16. Similar to the TGA results of cement mortar in the reference [64], the weight loss of dried RFA/CRFA between 30℃ and 150℃ was due to the water loss of C-S-H and ettringite. The weight loss between 370℃ and 430℃ was attributed to the decomposition of $Ca(OH)_2$. The weight loss between 450℃ and 720℃ was because of the decomposition of $CaCO_3$. It can be seen there were C-S-H, $Ca(OH)_2$, and ettringite in RFA. A small amount of $CaCO_3$ was also present in RFA because it was carbonated at a low level when stored in the air. Compared with the original RFA, the amount of $Ca(OH)_2$ and ettringite in RFA after soaking in SS solution was reduced. It indicates that part of the $Ca(OH)_2$ and ettringite in RFA were

dissolved and reacted with the SS solution. Moreover, the peak at about 75℃ was more obvious, which indicates total amount of C-S-H and C-(N)-A-S-H in RFA after soaking in SS solution. It can be inferred that SS solution can also penetrate into RFA and react with $Ca(OH)_2$ and ettringite, producing additional C-(N)-A-S-H.

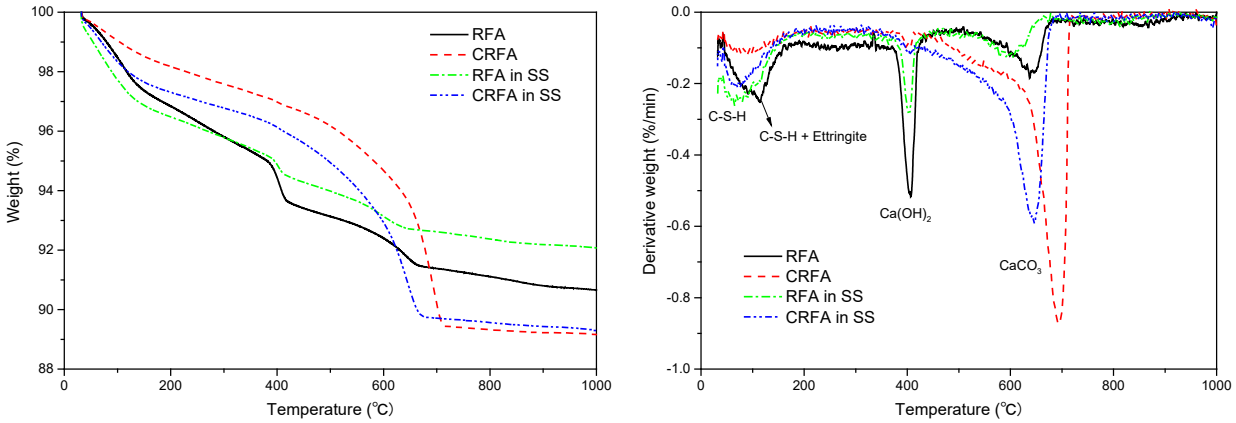

(a) TG (b) DTG

Fig. 16 TG and DTG of RFA/CRFA before and after soaking in SS solution

In CRFA, there was much more $CaCO_3$ than in RFA, including calcite and some amorphous $CaCO_3$ (450℃-600℃) [65-66]. At the same time, the amount of C-S-H, ettringite, and $Ca(OH)_2$ in CRFA was significantly reduced because of carbonation. Compared with the original CRFA, total amount of C-S-H and C-(N)-A-S-H in CRFA after soaking in SS solution was significantly increased. Moreover, the amount of $CaCO_3$ was reduced, and the peak corresponding to $CaCO_3$ shifted to a lower temperature which might be due to the reduced degree of crystallinity of $CaCO_3$ [67]. It can be inferred that SS solution might have penetrated into CRFA and reacted with amorphous $CaCO_3$, producing C-N-A-S-H and changing the crystal form of $CaCO_3$.

(3) SEM

The morphologies of RFA/CRFA before and after soaking in SS solution for 1 day are shown in Fig. 17. It shows that the main phases on the surface of RFA were C-S-H and ettringite. But there were no obvious $Ca(OH)_2$ crystals observed because the surface layer of RFA was carbonated when stored in air.

Regarding the RFA after soaking in SS solution, it was covered by C-(N)-A-S-H gel, which had been confirmed by EDS. The surface of CRFA was covered with calcite. However, besides calcite, there were some needle-shaped particles and larger size particles formed on the surface of CRFA after soaking in SS solution. As confirmed by EDS, the main elements of the needle-shaped particles and larger size particles were Ca, Si, Na, and O. It indicates that C-(N)-S-H was formed on the surface of CRFA after soaking in SS solution.

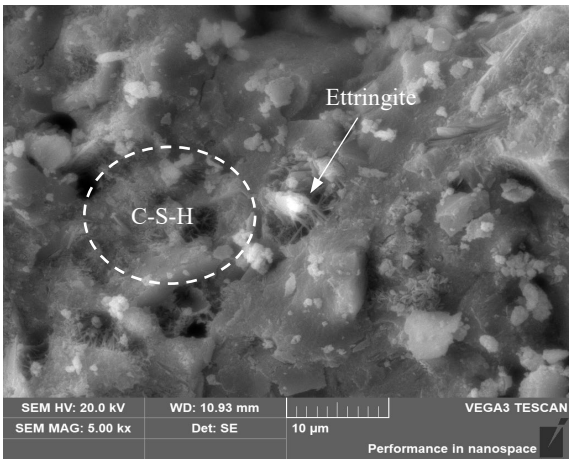

(a)RFA

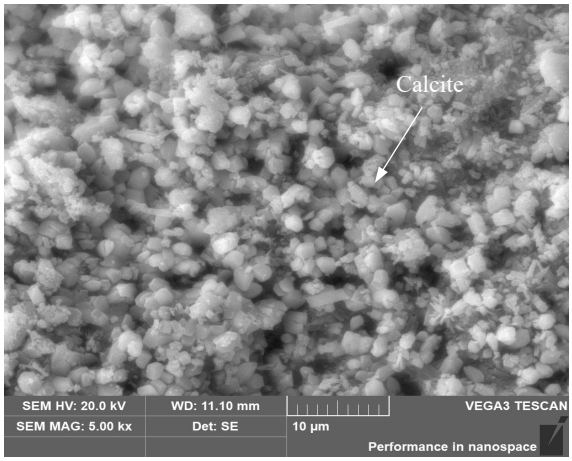

(b) CRFA

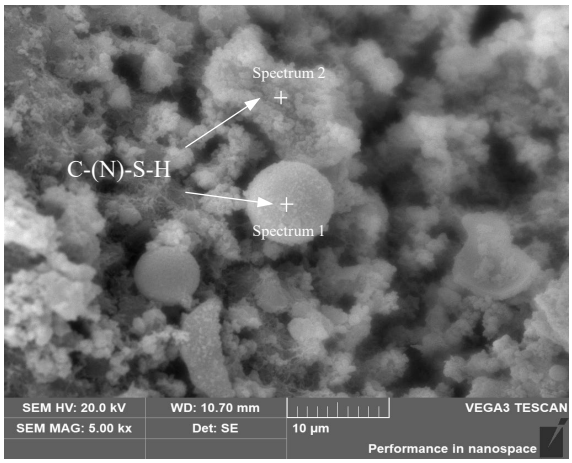

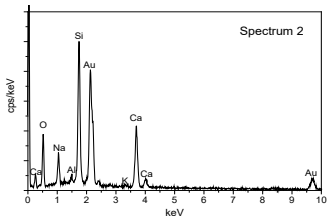

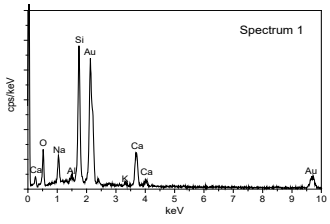

(c) RFA in SS

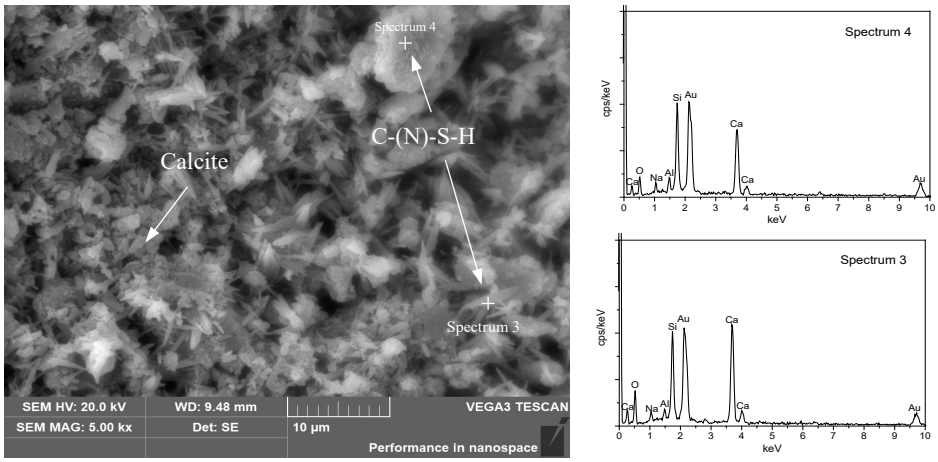

(d) CRFA in SS

Fig. 17 SEM images of RFA and CRFA before and after soaking in SS solution

(4) MIP

Pore size distribution of RFA/CRFA before and after soaking in SS solution are shown in Fig. 18. The porosity and the percentages of pores in different size ranges are listed in Table 7. Based on the influence of pore size on the performance of concrete, Wu and Lian [68] proposed to classify pores into four types: more harmful pore (>200 nm), harmful pores (50nm - 200nm), less harmful pores (20nm - 50nm), and harmless pores (< 20nm). It is observed that after using carbonation treatment, the porosity of RFA was reduced, the percentages of less harmful pores (20nm-50nm) and harmful pores (50nm-200nm) were both reduced while the percentage of the harmless pores (<20nm) was increased. Compared with the original RFA, the porosity of RFA after soaking in SS solution was obviously reduced. That was because SS solution penetrated into RFA and reacted with $Ca(OH)_2$ and calcium aluminate sulfate to form additional C-(N)-A-S-H. Alqarni et al. [69] also reported that the water absorption of recycled aggregate was reduced after soaking in SS solution. Compared to the original CRFA, the porosity of CRFA in the SS solution was slightly reduced. The percentages of harmless pores, less harmful pores, and harmful pores were all reduced due to the formation of additional C-(N)-S-H. But the percentage of more harmful pores (>200 nm) increased, and the volume of air holes (> several μm) was much higher. It might be due to the formation of gas when CRFA was soaked in SS solution.

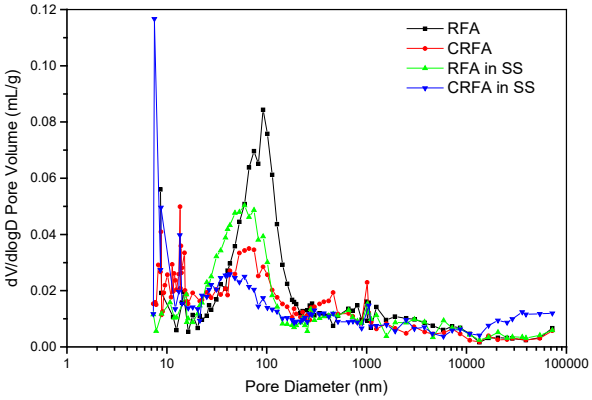

Fig. 18 Pore size distribution of RFA/CRFA before and after soaking in SS solution

Table 7 Analysis of pore structures of RFA/CRFA before and after soaking in SS solution

Sample ID	Porosity (%)	Percentage of pores in volume			
		< 20 nm (harmless pore)	20 ~ 50 nm (Less harmful)	50 ~ 200 nm (harmful)	> 200 nm (More harmful)
RFA	12.6	3.2%	42.5%	21.3%	33.0%
CRFA	10.6	17.2%	35.0%	11.6%	36.2%
RFA in SS	10.7	4.0%	50.5%	9.1%	36.4%
CRFA in SS	10.0	7.9%	32.7%	8.3%	51.1%

Combining the above XRD, TGA, SEM, and MIP results, it can be concluded that after soaking in SS solution, $Ca(OH)_2$ and ettringite in RFA were reduced while additional C-(N)-A-S-H was formed. It can be further confirmed that $Ca(OH)_2$ and ettringite in RFA were dissolved into SS solution and reacted with SS, producing C-(N)-A-S-H. Meanwhile, SS solution might also penetrate into RFA and reacted, producing C-(N)-A-S-H inside RFA. Regarding the CRFA after soaking in SS solution, the amount of C-S-H increased, while the amount of $CaCO_3$ was reduced and part of calcite was transformed into $CaCO_3$ with lower crystallinity. It can be speculated that SS might have reacted with the amorphous $CaCO_3$ in CRFA, producing additional C-(N)-S-H inside CRFA.

3.4.3 Characteristics of SS solution after soaking with RFA and CRFA

(1) Chemical composition

The chemical compositions of SS solution before and after soaking with RFA and CRFA are shown in Table 8. The main chemical compositions of SS solution in SS-control, SS-RFA, and SS-CRFA were H_2O, Na_2O, and SiO_2, while other oxides were very limited. It means the calcium and aluminum that were

dissolved from RFA had reacted and precipitated in the C-(N)-A-S-H gel. Compared with SS-control, both the Na_2O and SiO_2 contents in the SS solution of SS-RFA were reduced. Also, the SiO_2/Na_2O ratio of SS-RFA was reduced. That is because part of SS had reacted with $Ca(OH)_2$ and calcium aluminate sulfate. Compared with SS-control, both the Na_2O and SiO_2 contents in SS-CRFA were also reduced. It is because part of SS had reacted with CRFA.

Table 8 Chemical compositions of SS solution before and after soaking with RFA/CRFA

Compositions of SS solution	SS-control (% in mass)	SS-RFA (% in mass)	SS-CRFA (% in mass)
Na_2O	2.55	2.34	2.29
SiO_2	4.34	3.21	3.83
Cl	0	0.045	0
K_2O	0.04	0.05	0.05
CaO	0.009	0.008	0.007
H_2O	93.004	94.4	93.8

(2) pH value

The pH values of SS solution before and after soaking with RFA and CRFA are displayed in Table 9. It can be observed that the pH of SS solution in SS-RFA was higher than that in SS-control and it increased with the increase of soaking time. It means the alkali concentration increased significantly after incorporating RFA and CRFA in the SS solution. e.g., after soaking for 4 hours, the pH value increased from 12.31 to 12.63, which means the concentration of hydroxide increased by 109%. It indicates additional hydroxide was produced after soaking RFA in the SS solution. It can be speculated that sodium hydroxide might be also produced when the $Ca(OH)_2$ in RFA reacted with SS. On the contrary, the pH of SS solution in SS-CRFA was lower than the SS-control and it decreased with the increase of soaking time. e.g., after soaking for 1 day, the pH value increased from 12.24 to 12.08, which means the concentration of hydroxide decreased by 45%. It may be because the acidic substance in CRFA (namely silica gel) also participated in the reaction between CRFA and SS solution, which reduced the alkalinity of the SS solution.

Table 9 pH values of SS solution before and after soaking with RFA and CRFA

pH of SS solution	SS-control	SS-RFA	SS-CRFA
After 4 hours	12.31	12.63	12.23
After 1 day	12.29	12.68	12.16
After 2 days	12.28	12.81	12.14
After 4 days	12.25	12.89	12.09
After 7 days	12.24	13.00	12.08

(3) ATR-FTIR

The ATR-FTIR spectra of SS solution before and after soaking with RFA and CRFA are demonstrated in Fig. 19. According to the literature [70], in the ATR-FTIR spectra, the peak at 3310 cm^{-1} is attributed to Si-OH and adsorbed water functional group, the peak at 1640 cm-1 is assigned to O-H vibration of absorbed water, the peaks at 1410 cm^{-1} is due to vibrations of carbonate, and the peaks at 1010 cm-1 is assigned to the asymmetric stretching vibration of Si-O-Si in SS. Comparing the ATR-FTIR spectra of SS solution in SS-control, SS-RFA, and SS-CRFA, no significant difference was found. In particular, the weak peak at 1410cm^{-1} indicated that there was carbonate in SS-control, due to the reaction between CO_2 and SS when stored in air. In SS-CRFA, the peak at 1420cm^{-1} was similar to that in SS-control. It indicates that no additional carbonate was produced in the reaction between CRFA and SS solution. Combining the bubbles observed in the SS-CRFA, it can be inferred that CO_2 gas was formed when SS reacted with the silica gel and $CaCO_3$ in CRFA.

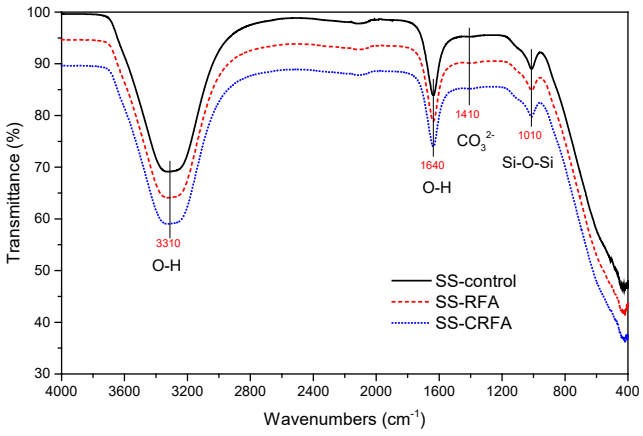

Fig. 19 ATR-FTIR spectra of SS solutions before and after soaking with RFA and CRFA

3.4.4 Discussion on chemical reactions of SS solution with RFA/CRFA

Combing the above results, the chemical reactions of SS solution with RFA/CRFA can be summarized as follows. When RFA was soaked in SS solution, $Ca(OH)_2$ in RFA was dissolved into SS solution and reacted with SS, producing C-(N)-S-H and sodium hydroxide. Meanwhile, calcium aluminate sulfate (ettringite) and Mg^{2+} were also dissolved from RFA into SS solution and reacted with SS, which formed C-(N)-A-S-H and hydrotalcite. Because of these reactions, C-(N)-A-S-H gel (including C-(N)-S-H) was formed in SS solution and the pH value of SS solution was increased. Besides, RFA itself became denser because SS solution penetrated into RFA and similar reactions occurred inside RFA. When CRFA was soaked in SS solution, SS solution penetrated into CRFA and reacted with amorphous $CaCO_3$ and silica in CRFA, producing C-(N)-S-H and CO_2 gas. Meanwhile, part of calcite was transformed to $CaCO_3$ with lower crystallinity. As a result, the pH value of the SS solution was decreased.

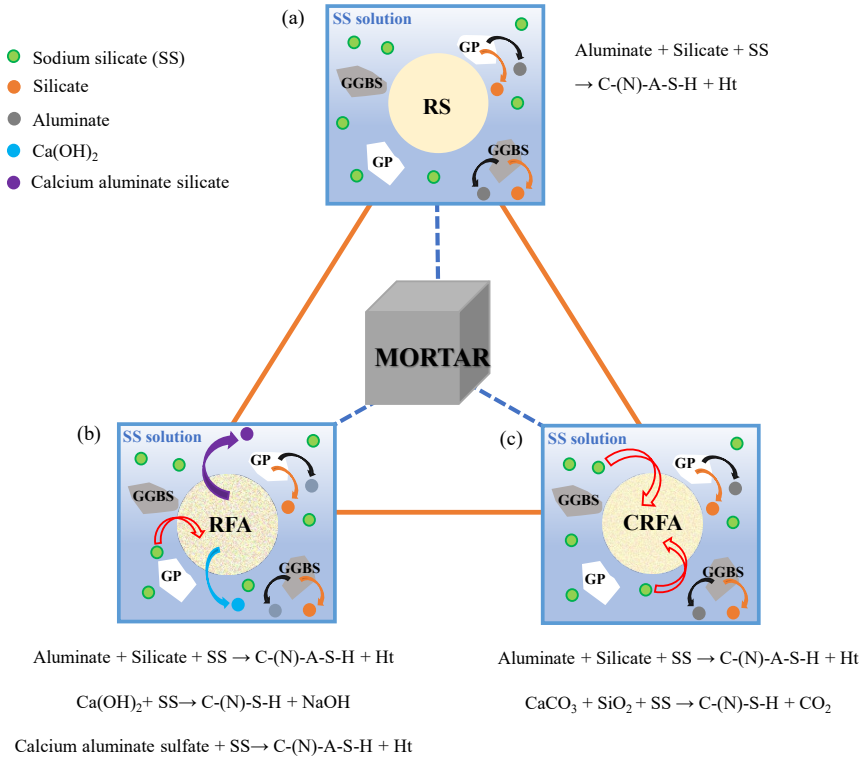

Fig. 20 Substances migration and reactions in AASGMs. (a) M-control; (b) M-100% RFA; (c) M-100%CRFA

4. Discussions

Based on the above test results, the reactions in AASGMs with RFA and CRFA and the mechanisms of performance change after incorporating RFA/CRFA are discussed below.

The schematics of substance migration and reactions in AASGMs with RFA/CRFA are illustrated in Fig. 20. In the M-Control, the aluminosilicate is firstly depolymerized, while the aluminate and silicate are dissolved from GGBS and GP particles into the alkali solution. Then, the aluminate and silicate in the SS solution were polymerized again to form new aluminosilicate gel (C-(N)-A-S-H) and hydrotalcite (Ht) [62][71].

As shown in Fig.20(b), when RFA was incorporated in AASGM, $Ca(OH)_2$ and calcium aluminate sulfate in RFA were also dissolved. Then, the $Ca(OH)_2$ reacted with SS to produce additional C-(N)-S-H gel and NaOH, while the calcium aluminate sulfate reacted with SS to produce additional C-(N)-A-S-H gel. It was equivalent to increasing the alkali concentration or decreasing the SiO_2/Na_2O ratio of the activator. As a result, the polymerization reaction in AASGM was accelerated after incorporating RFA. Generally, higher alkali concentration can accelerate the polymerization reactions of alkali-activated materials at a medium level of alkali concentration and increase the strength [46][72]. That is why the flow value and initial setting time of AASGM decreased with the increase of RFA content. Also, the microhardness of new paste in AASGM was increased with the increase of RFA content. Due to the enhanced new paste, the 28-day compressive strength of AASGM increased with RFA content when it was less than 50%. But, because RFA was weaker than the river sand, it also had a negative effect on the compressive strength of AASGM. When too much RFA was incorporated, the compressive strength of AASGM decreased. Because of the reduced SiO_2/Na_2O ratio of the activator caused by incorporating RFA, the drying shrinkage of AASGM decreased with the increase of RFA content. That is because the pore structures of alkali-activated materials are refined when increasing the SiO_2/Na_2O ratio of the activator [54]. Generally, the autogenous shrinkage of AAM increased with the increase of the alkali concentration of the activator [73]. But the autogenous shrinkage of AASGM decreased with RFA content although the alkali concentration increased. It indicates

650 that the decreased autogenous shrinkage of AASGM after adding RFA was not due to the reaction change.
651 It should be because of the internal curing effect of RFA, which had been reported as the main reason for
652 decreased autogenous shrinkage of OPC-based concrete or mortar prepared with RFA [50].

653 As shown in Fig.20(c), when CRFA was incorporated in AASGM, the SS solution penetrated into CRFA
654 and reacted with amorphous calcium carbonate and silica gel, producing C-(N)-S-H and CO_2 gas. This
655 reaction may have consumed part of the alkali and thus decreased the alkali concentration of the activator,
656 which decelerated the reactions that happened in the M-control. That is why the flow value and setting time
657 of AASGM increased with the increase of CRFA content. Also, the microhardness of new paste in AASGM
658 decreased with the increase of RFA content. As a result, the compressive strength of AASGM decreased
659 with the increase of CRFA content and the compressive strength of AASGM with CRFA was lower than
660 AASGM with the same amount of RFA although CRFA was stronger than RFA. In addition, because
661 incorporating CRFA reduced the alkali concentration of the activator, the formation of C-(N)-A-S-H gel
662 was decelerated. As a result, incorporating CRFA led to reduced autogenous shrinkage and drying
663 shrinkage of AASGM, and incorporating CRFA brought in a larger reduction than adding the same amount
664 of RFA. To confirm the reduced alkali concentration was the reason for the changed performance when
665 incorporating CRFA, more activator was added based on the mix M-100%CRFA. It showed that when the
666 SS to binder ratio was 0.2, the 7-day compressive strength of M-100%CRFA was increased to 19.0 MPa,
667 which was close to that of M-50%CRFA. The results indicated that the explanation was reasonable.

668 # 5. Conclusions

669 In this study, the influences of using recycled fine aggregate (RFA) and carbonated RFA (CRFA) as
670 partial or full replacement of river sand on microstructural and macro properties of alkali-activated slag and
671 glass powder mortar (AASGM) were investigated. Also, the reaction mechanisms of AASGMs with RFA
672 and CRFA were studied. Based on the test results and discussions above, the following conclusions can be
673 drawn.

(1) With the increase in RFA content from 0% to 100%, the flow value of AASGM decreased from 240mm to 145mm, the initial setting time was shortened by 44%, the autogenous shrinkage at 7 days decreased by 82%, drying shrinkage of AASGM at 25 days decreased by 31%, and the microhardness at 28 days increased by 30%. Moreover, the compressive strength of AASGM at 28 days firstly increased with RFA content when it was less than 50% due to the enhanced new paste. But further increasing RFA content, the compressive strength of AASGM at 28 days decreased because of the negative effect of the weaker RFA than river sand. Overall, the use of RFA as a replacement of river sand can effectively improve the studied performance of alkali-activated mortar. However, the effects of RFA on long-term properties of AASGM are still unknown, which needs further studies.

(2) The influences of RFA on the properties of AASGM was different from its influences on OPC-based materials, in which the performance decreased with increase of RFA content. That is because the $Ca(OH)_2$ and calcium aluminate sulfate in RFA could be dissolved and reacted with the sodium silicate (SS) activator, which produced additional sodium-containing calcium aluminosilicate hydrates (C-(N)-A-S-H) in the new paste of AASGM and increased the alkali concentration of activator. As a result, the polymerization reaction of AASGM was accelerated after incorporating RFA.

(3) With the increase of CRFA content from 0% to 100%, the flow value of AASGM increased from 240mm to 270mm, the final setting time increased by 37%, and the compressive strength of AASGM decreased by 97%. These features were contrary to the case of using RFA in AASGM. Moreover, the autogenous shrinkage and drying shrinkage of AASGM with CRFA showed a larger decrease than using the same amount of RFA. Overall, CRFA had negative effect on the performance of AASGM and more alkali activator need to be added to increase the performance, which will increase the cost of the material. Therefore, CRFA was not recommended to use in AASGM.

(4) The influences of CRFA on the properties of AASGM was also different from its influences on OPC-based materials, in which the performance is improved comparing to using same amount of RFA. That was because when CRFA was incorporated in AASGM, the amorphous calcium carbonate and silica in CRFA

699 reacted with SS, which produced C-(N)-S-H and CO_2 gas. This reaction reduced the alkali concentration of
700 the activator, which decelerated the polymerization reaction of AASGM.

701 6. Acknowledgement

702 The authors would like to thank the Research Grants Council GRF funding of Hong Kong for financial
703 support.

704 7. References

[1] R.M. Andrew, Global CO_2 emissions from cement production. Earth System Science Data 10 (2018) 195–217.

[2] L.K. Turner, F.G. Collins, Carbon dioxide equivalent (CO2-e) emissions: A comparison between geopolymer and OPC cement concrete, Construction and Building Materials 43 (2013) 125–130.

[3] Y.H. M. Amran, R. Alyousef, H. Alabduljabbar, M. El-Zeadani, Clean production and properties of geopolymer concrete; A review. Journal of Cleaner Production 251 (2020) 119679.

[4] B. Singh, G. Ishwarya, M. Gupta, S.K. Bhattacharyya, Geopolymer concrete: A review of some recent developments. Construction and Building Materials 85 (2015) 78-90.

[5] M. Amran, S.S. Huang, S. Debbarma, R. S.M. Rashid, Fire resistance of geopolymer concrete: A critical review. Construction and Building Materials 324 (2022) 126722.

[6] B. Wang, L. Yan, Q. Fu, B. Kasal, A Comprehensive Review on Recycled Aggregate and Recycled Aggregate Concrete. Resources, Conservation and Recycling 171(2021) 105565.

[7] J. Xiao, W. Li, Y. Fan, X. Huang, 2012. An overview of study on recycled aggregate concrete in China (1996–2011). Construction and Building Materials 31 (2012) 364–383.

[8] M. Upshaw, C. S. Cai, Critical Review of Recycled Aggregate Concrete Properties, Improvements, and Numerical Models. Journal of Materials in Civil Engineering 32(11) (2020) 03120005.

[9] Z. Ma, J. Shen, C. Wang, H. Wu, Characterization of sustainable mortar containing high-quality recycled manufactured sand crushed from recycled coarse aggregate. Cement and Concrete Composites, 132 (2022) 104629.

[10] H. Zhang, T. Ji, X. Zeng, Z. Yang, X. Lin, Y. Liang, Mechanical behavior of ultra-high performance concrete (UHPC) using recycled fine aggregate cured under different conditions and the mechanism based on integrated microstructural parameters. Construction and Building Materials 192 (2018) 489–507.

[11] H. Zhang, J. Xiao, Y. Tang, Z. Duan, C.S. Poon, Long-term shrinkage and mechanical properties of fully recycled aggregate concrete: Testing and modelling. Cement and Concrete Composites 130(2022)104527.

[12] J. Xiao. Recycled Aggregate Concrete Structures. Berlin: Springer-Verlag, 2018.

[13] P. Ren, B. Li, J.G. Yu, T.C. Ling, Utilization of recycled concrete fines and powders to produce alkali-activated slag concrete blocks. Journal of Cleaner Production 267 (2020) 122115.

[14] N.K. Lee, S.Y. Abate, H. Kim, Use of recycled aggregates as internal curing agent for alkali-activated slag system. Construction and Building Materials 159 (2018) 286-296.

[15] Y. Hu, Z. Tang, W. Li, Y. Li, V.W.Y. Tam, Physical-mechanical properties of fly ash/GGBFS geopolymer composites with recycled aggregates. Construction and Building Materials 226 (2019) 139-151.

[16] J. Huang, C. Zou, D. Sun, B. Yang, J.Yan, Effect of recycled fine aggregates on alkali-activated slag concrete properties. Structures 30 (2021) 89-99.

[17] Z. Tang, W.G. Li, P.R. Li, S.P. Shah, Durability of Sustainable Construction Materials with Solid Wastes [M], Springer Nature Singapore Pte Ltd. (2020). https://10.1007/978-981-13-7603-0_1.

[18] Z. Tang, W. Li, V.W.Y Tam, Mechanical Behavior of CFRP-Confined Recycled Fly Ash/Slag Based Geopolymer (July 20, 2019). Abstract Proceedings of 2019 International Conference on Resource Sustainability - Cities (icRS Cities), https://ssrn.com/abstract=3423191.

[19] Z. Tang, W. Li, Q. Peng, V.W.Y Tam, K. Wang, Study on the failure mechanism of geopolymeric

recycled concrete using digital image correlation method, Journal of Sustainable Cement-Based Materials 11(2) (2022)113-126, DOI: 10.1080/21650373.2021.1897706.

[20] C. Liang, B. Pan, Z. Ma, Z. He, Z. Duan. Utilization of CO2 curing to enhance the properties of recycled aggregate and prepared concrete: A review. Cement and Concrete Composites 105 (2020) 103446.

[21] L. Li, D. Xuan, A.O. Sojobi, S. Liu, C.S. Poon, Efficiencies of carbonation and nano silica treatment methods in enhancing the performance of recycled aggregate concrete. Construction and Building Materials 308 (2021) 125080.

[22] X. Fang, D. Xuan, C.S. Poon, Empirical modelling of CO_2 uptake by recycled concrete aggregates under accelerated carbonation conditions. Materials and Structures 50 (2017) 200.

[23] L. Li, J. Xiao, D. Xuan, C.S. Poon, Effect of carbonation of modeled recycled coarse aggregate on the mechanical properties of modeled recycled aggregate concrete. Cement and Concrete Composites 89 (2018) 169-180.

[24] L. Li, C.S. Poon, J. Xiao, D. Xuan, Effect of carbonated recycled coarse aggregate on the dynamic compressive behavior of recycled aggregate concrete. Construction and Building materials 151 (2017) 52-62.

[25] J. Zhang, C. Shi, Y. Li, X. Pan, C.S. Poon, Z. Xie, Performance Enhancement of Recycled Concrete Aggregates through Carbonation. Journal of Materials in Civil Engineering 11(27)(2015) 04015029.

[26] J. Zhang, C. Shi, J. Li, X. Pan, C.S. Poon, Z. Xie, Influence of carbonated recycled concrete aggregate on properties of cement mortar. Construction and Building Materials 98 (2015) 1-7.

[27] B.J. Zhan, D.X. Xuan, C.S. Poon, K.L. Scrivener, Characterization of interfacial transition zone in concrete prepared with carbonated modeled recycled concrete aggregates. Cement and Concrete Research 136 (2020) 106175.

[28] Y. Jeong, W.S. Yum, J. Moon, J. E.Oh, Utilization of precipitated CaCO3 from carbon sequestration of industrially emitted CO2 in cementless CaO-activated blast-furnace slag binder system. Journal of Cleaner Production 166 (2017) 649-659.

[29] R. Firdous, T. Hirsch, D. Klimm, B. Lothenbach, D. Stephan, Reaction of calcium carbonate minerals in sodium silicate solution and its role in alkali-activated systems, Minerals Engineering 165 (2021) 106849.

[30] P. He, B. Zhang, J.X. Lu, C.S. Poon, Reaction mechanisms of alkali-activated glass powder-ggbs-CAC composites. Cement and Concrete Composites 122 (2021) 104143.

[31] L. Li, J.X. Lu, B. Zhang, C.S. Poon, Rheology behavior of one-part alkali activated slag/glass powder (AASG) pastes. Construction and Building Materials 258 (2020) 120381.

[32] P. He, B. Zhang, S. Yang, H. A. Ali, J.X. Lu, C.S. Poon, Recycling of Glass Cullet and Glass Powder in Alkali-Activated Cement: Mechanical Properties and Alkali–Silica Reaction. Waste and Biomass Valorization 11 (2020) 7159–7169.

[33] P. Shoaei, F. Ameri, H.R. Musaeei, T. Ghasemi, C.C. Ban., Glass powder as a partial precursor in Portland cement and alkali-activated slag mortar: A comprehensive comparative study. Construction and Building Materials 251 (2020) 118991.

[34] Lin-hu Yang, Zhu Han, Cheng-fang Li, Strengths and flexural strain of CRC specimens at low temperature. Construction and Building Materials 25(2)(2011)906-910.

[35] Z. Abdollahnejad, T. Luukkonen, M. Mastali, C. Giosue, O. Favoni, M.L. Ruello, M. Illikainen, Microstructural analysis and strength development of one-part alkali-activated slag/ceramic binders under different curing regimes. Waste and biomass valorization 11(6) (2020)3081-3096.

[36] F.G. Collins, J.G. Sanjayan, Workability and mechanical properties of alkali activated slag concrete, Cement and Concrete Research 29(3) (1999) 455-458.

[37] H. Sun, Z. Ren, S. A. Memon, D. Zhao, X. Zhang, D. Li, F. Xing, Investigating drying behavior of cement mortar through electrochemical impedance spectroscopy analysis, Construction and Building Materials135(2017) 361-368.

[38] L. Li, D. Xuan, A.O. Sojobi, S.i Liu, S.H. Chu, C.S. Poon, Development of nano-silica treatment methods to enhance recycled aggregate concrete. Cement and Concrete Composites 118(6) (2021)103963.

[39] L. Li, D. Xuan, S.H. Chu, J.X. Lu, C.S. Poon, Efficiency and mechanism of nano-silica pre-spraying treatment in performance enhancement of recycled aggregate concrete. Construction and Building Materials 301(6) (2021)124093.

[40] C.S. Poon, Z.H. Shui, L. Lam, H. Fok, S.C. Kou, Influence of moisture states of natural and recycled aggregates on the slump and compressive strength of concrete. Cement and Concrete Research 34 (1) (2004) 31–36.

[41] S. Choi, K. Lee, Influence of Na2O Content and Ms (SiO_2/Na_2O) of Alkaline Activator on Workability and Setting of Alkali-Activated Slag Paste. Materials 12(13)(2019) 2072.

[42] X. Jia, T.C. Ling, H. Mehdizadeh, K. H. Mo, Impact of CO2 curing on the microhardness and strength of 0.35 w/c cement paste: Comparative study of internal/surface layers, Journal of Materials Research and Technology 9(5)2020 11849-11860.

[43] B. Lu, C. Shi, J. Zheng, T.C. Ling, 11 - Carbon dioxide sequestration on recycled aggregates, Editors: F. P. Torgal, C. Shi, A. P. Sanchez, In Woodhead Publishing Series in Civil and Structural Engineering, Carbon Dioxide Sequestration in Cementitious Construction Materials, Woodhead Publishing, 2018, 247-277.

[44] Z. Tang, W. Li, Chapter 21 - Utilization of recycled aggregate in geopolymer concrete development: A case study, Editor(s): Daniel C.W. Tsang, Lei Wang, Low Carbon Stabilization and Solidification of Hazardous Wastes, Elsevier, 2022: 343-354. https://doi.org/10.1016/B978-0-12-824004-5.00015-3.

[45] S. Hanjitsuwan, S. Hunpratub, P. Thongbai, S. Maensiri, V. Sata, P. Chindaprasirt, Effects of NaOH concentrations on physical and electrical properties of high calcium fly ash geopolymer paste. Cement and Concrete Composites 45 (2014) 9–14.

[46] H. Taghvayi, K. Behfarnia, M. Khalili, The effect of alkali concentration and sodium silicate modulus on the properties of alkali-activated slag concrete. Journal of Advanced Concrete Technology 16 (2018) 293–305.

[47] Z. Zhao, S. Remond, D. Damidot, W. Xu, Influence of fine recycled concrete aggregates on the properties of mortars. Construction and Building Materials 81 (2015) 179–186.

[48] L. Li, B.J. Zhan, J.X. Lu, C.S. Poon, Systematic evaluation of the effect of replacing river sand by different particle size ranges of fine recycled concrete aggregates (FRCA) in cement mortars. Construction and Building materials 209(10) (2019)147-155.

[49] Q. Liu, J. Zhang, Y. Su, X. Lu. Variation in Polymerization Degree of C-A-S-H Gels and Its Role in Strength Development of Alkali-activated Slag Binders. Journal of Wuhan University of Technology-Mater. Sci. Ed 36 (2021) 871–879.

[50] Y. Mao, J. Liu, C. Shi, Autogenous shrinkage and drying shrinkage of recycled aggregate concrete: A review. Journal of Cleaner Production 295 (2021) 126435.

[51] H. Zhang, Y.Y. Wang, D. E. Lehman, Y.Geng, Autogenous-shrinkage model for concrete with coarse and fine recycled aggregate, Cement and Concrete Composites 111(2020)103600.

[52] G. Fang, H. Bahrami, M. Zhang, Mechanisms of autogenous shrinkage of alkali-activated fly ash-slag pastes cured at ambient temperature within 24 h. Construction and Building Materials 171 (2018) 377-387.

[53] A.R. Sakulich, D.P. Bentz, Mitigation of autogenous shrinkage in alkali activated slag mortars by internal curing. Materials and Structures 46 (2013) 1355–1367.

[54] X. Gao, Q.L. Yu, H.J.H. Brouwers, Assessing the porosity and shrinkage of alkali activated slag-fly ash composites designed applying a packing model. Construction and Building Materials 119 (2016) 175-184.

[55] H. Taghvayi, K. Behfarnia, M. Khalili, The Effect of Alkali Concentration and Sodium Silicate Modulus on the Properties of Alkali-Activated Slag Concrete. Journal of Advanced Concrete Technology 16 (2018) 293-305.

[56] B. Fu, Z. Cheng, J. Han, N. Li, Understanding the Role of Metakaolin towards Mitigating the Shrinkage Behavior of Alkali-Activated Slag. Materials 14 (2021) 6962.

[57] F. Collinsa, J.G. Sanjayan, Effect of pore size distribution on drying shrinkage of alkali-activated slag concrete. Cement and Concrete Research 30 (2000) 1401– 1406.

[58] H. Wang, L. Wang, W. Shen, K. Cao, L. Sun, P. Wang, L. Cui, Compressive Strength, Hydration and Pore Structure of Alkali-Activated Slag Mortars Integrating with Recycled Concrete Powder as Binders. KSCE Journal of Civil Engineering volume 26 (2022)795–805.

[59] B.S. Gebregziabiher, R. Thomas, S. Peethamparan, Very early-age reaction kinetics and microstructural development in alkali-activated slag. Cement and Concrete Composites 55 (2015) 91–102.

[60] B.K. Darshan, S. Peethamparan, Quantification of drying shrinkage in alkali activated slag mortars and validating the efficiency of various shrinkage mitigation methods. Transportation Research Board 96th Annual Meeting, Washington DC, United States, 2017.

[61] P. Giannaros, A. Kanellopoulos, A. Al-Tabbaa, Sealing of cracks in cement using microencapsulated sodium silicate. Smart Materials and Structures 25(8) (2016) 84005.

[62] S.D. Wang, K.L. Scrivener, Hydration products of alkali activated slag cement. Cement and Concrete Research, 25(3) (1995) 561-571.

[63] Y. Zuo, M. Nedeljković, G. Ye, Coupled thermodynamic modelling and experimental study of sodium hydroxide activated slag, Construction and Building Materials 188(2018)262-279.

[64] A.V. Soin, L.J.J. Catalan, S.D. Kinrade, A combined QXRD/TG method to quantify the phase composition of hydrated Portland cements, Cement and Concrete Research 48(2013)17-24.

[65] P. Shen, Y. Zhang, Y. Jiang, B. Zhan, J.X. Lu, S. Zhang, D. Xuan, C.S. Poon, Phase assemblance evolution during wet carbonation of recycled concrete fines. Cement and Concrete Research 154 (2022) 106733.

[66] P. Shen, Y. Sun, S. Liu, Y. Jiang, H. Zheng, D. Xuan, J. Lu, C.S. Poon, Synthesis of amorphous nano-silica from recycled concrete fines by two-step wet carbonation. Cement and Concrete Research 147 (2021) 106526.

[67] V. Rostami, Y. Shao, A.J. Boyd, Z. He, Microstructure of cement paste subject to early carbonation curing. Cement and Concrete Research 42(1)(2012) 186-193.

[68] Z.W. Wu, H.Z. Lian. High performance concrete. Beijing: Railway Press of China, 1999. (in Chinese).

[69] A.S. Alqarni, H. Abbas, K.M. Al-Shwikh, Y.A. Al-Salloum, Treatment of recycled concrete aggregate to enhance concrete performance. Construction and Building Materials 307 (2021)124960

[70] P. Worathanakul, W. Payubnop, A. Muangpet, Characterization for Post-treatment Effect of Bagasse Ash for Silica Extraction. International Journal of Chemical and Molecular Engineering 3(8)(2009) 398-400.

[71] R.J. Myers, S. A. Bernal, J.L. Provis, Phase diagrams for alkali-activated slag binders. Cement and Concrete Research 95 (2017) 30–38.

[72] S. Hanjitsuwan, S. Hunpratub, P. Thongbai, S. Maensiri, V. Sata, P. Chindaprasirt, Effects of NaOH concentrations on physical and electrical properties of high calcium fly ash geopolymer paste. Cement and Concrete Composites 45 (2014) 9–14.

[73] D. B. Kumarappa, S. Peethamparan, M. Ngami, Autogenous shrinkage of alkali activated slag mortars: Basic mechanisms and mitigation methods. Cement and Concrete Research 109 (2018) 1-9.